



저작자표시-비영리-변경금지 2.0 대한민국

이용자는 아래의 조건을 따르는 경우에 한하여 자유롭게

- 이 저작물을 복제, 배포, 전송, 전시, 공연 및 방송할 수 있습니다.

다음과 같은 조건을 따라야 합니다:



저작자표시. 귀하는 원저작자를 표시하여야 합니다.



비영리. 귀하는 이 저작물을 영리 목적으로 이용할 수 없습니다.



변경금지. 귀하는 이 저작물을 개작, 변형 또는 가공할 수 없습니다.

- 귀하는, 이 저작물의 재이용이나 배포의 경우, 이 저작물에 적용된 이용허락조건을 명확하게 나타내어야 합니다.
- 저작권자로부터 별도의 허가를 받으면 이러한 조건들은 적용되지 않습니다.

저작권법에 따른 이용자의 권리는 위의 내용에 의하여 영향을 받지 않습니다.

이것은 [이용허락규약\(Legal Code\)](#)을 이해하기 쉽게 요약한 것입니다.

[Disclaimer](#)

Thesis of Degree of Master of Natural Science

**Improved Stability of Perovskite Solar
Cells with a Surface Treated Electron
Transport Layer**



By

Pesi Mwitumwa Hangoma
Department of Physics
The Graduate School
Pukyong National University

August 2017

Improved Stability of Perovskite Solar Cells with a Surface Treated Electron Transport Layer

(전자수송층의 표면특성 조절을 통한
페로브스카이트 태양전지의 안정성 향상연구)

Advisor: Prof. Sung Heum Park



By

Pesi Mwitumwa Hangoma

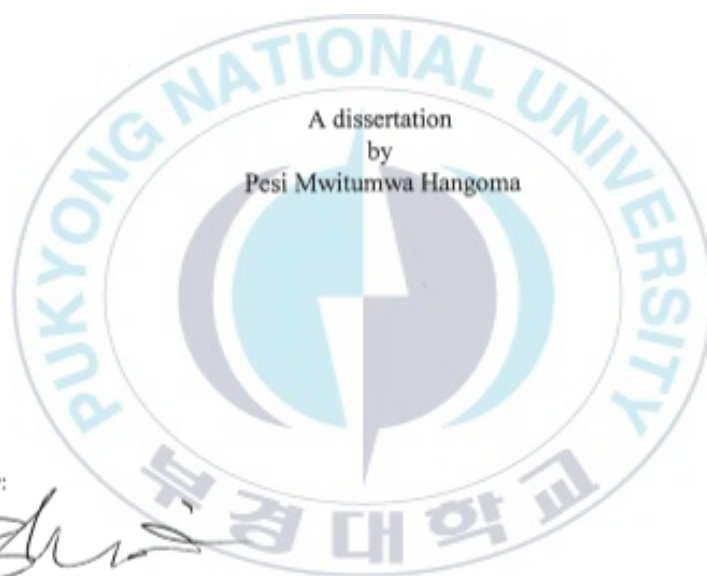
A thesis submitted in partial fulfillment of the requirements
for the degree of

Master of Natural Science

in Department of Physics, The Graduate School,
Pukyong National University

August 2017

Improved Stability of Perovskite Solar Cells with a Surface Treated Electron
Transport Layer



A dissertation
by
Pesi Mwitumwa Hangoma

Approved by:

A handwritten signature in black ink, appearing to be 'Byung Chun Choi', written over a horizontal line.

(Chairman) Byung Chun Choi

A handwritten signature in black ink, appearing to be 'Jae-Won Jang', written over a horizontal line.

(Member) Jae-Won Jang

A handwritten signature in black ink, appearing to be 'Sung Heon Park', written over a horizontal line.

(Member) Sung Heon Park

August 2017

Content

Abstract.....	Vii
Chapter 1. Introduction	1
1.1 RESEARCH BACKGROUND.....	1
1.2 PEROVSKITE MATERIAL.....	5
1.3 MECHANISM OF THE PEROVSKITE SOLAR CELLS.....	9
1.4 DEGRADATION IN PEROVSKITE SOLAR CELLS.....	11
1.5 DEVELOPMENT OF THE STABILITY OF PEROVSKITE SOLAR CELLS.....	14
Chapter 2. Influence of the Electrode on Device Stability.....	16
2.1 DEVICE DEGRADATION DUE TO ALUMINIUM ELECTRODES.....	16
2.2 SURFACE MORPHOLOGY.....	20
2.3 X-RAY DIFFRACTION.....	22
2.4 ELECTRODE-INFLUENCED DEGRADATION MECHANISM	24

Chapter 3. Surface Treatment of the Electron Transport Layer.....	28
3.1 STEARIC ACID AND ITS APPLICATIONS.....	28
3.2 DEVICE FABRICATION AND SURFACE TREATMENT...31	
3.3 ADSORPTION OF STEARIC ACID ON THE SURFACE.....35	
3.4 WATER RESISTIVITY OF THE TREATED SURFACE.....38	
Chapter 4. Results and Discussion.....	41
4.1 SCANNING ELECTRON MICROSCOPE.....	41
4.2 ATOMIC FORCE MICROSCOPY.....	43
4.3 FOURIER TRANSFORM INFRA-RED SPECTROSCOPY ...45	
4.4 X-RAY DIFFRACTION.....	47
4.5 UV-VISIBLE ABSORPTION.....	49
4.6 J-V CHARACTERISTIC OF TREATED DEVICES.....	52
4.7 DEVICE PERFORMANCE IN AIR.....	60
Chapter 5. Conclusion.....	64
References List.....	66
Acknowledgements.....	73

List of Figures

Figure 1. Crystal Structure of a perovskite unit cell.....	7
Figure 2. Photovoltaic solar cells' development chart with time.....	8
Figure 3. Device architecture of a) planar heterojunction p-i-n layered device and b) mechanism of perovskite solar cell device.....	10
Figure 4. Graph of device efficiency with time	18
Figure 5. J-V curves of a) original device, b) device exposed to air and c) device with redeposited electrodes.....	19
Figure 6. Optical microscope and top-view SEM images of Aluminum electrode surface under different conditions.....	21
Figure 7. XRD patterns of glass/ITO/ PEDOT:PSS/CH ₃ NH ₃ PbI ₃ /PCBM structured film covered by Aluminum electrodes	23
Figure 8. Illustration of the Formation and Removal of Aluminum iodide from the perovskite device.....	26
Figure 9. J -V characteristics and PCE's of devices with and without electrode redepositon	27
Figure 10. Chemical structure of Stearic acid, Ethylenediamine and PCBM.....	30
Figure 11. Schematic of the fabrication and adsorption of Stearic acid on perovskite device with a glass/ITO/PEDOT:PSS/ CH ₃ NH ₃ PbI ₃ / /PCBM/Al structure.....	34

Figure 12. Contact angle for (a) a non-treated film and (b) treated film 6g/ml Stearic acid in IPA solution and (0.06%) Ethylenediamine.....	39
Figure 13. Water resistivity of non-treated and treated glass/ITOPEDOT:PSS /CH ₃ NH ₃ PbI ₃ /PCBM structured films immersed in water.....	40
Figure 14. Top-view SEM images of the surface morphology of glass/ITO/ PEDOT:PSS/ CH ₃ NH ₃ PbI ₃ /PCBM structured films.....	42
Figure 15. AFM of the surface topography of glass/ITO/ PEDOT:PSS /CH ₃ NH ₃ PbI ₃ /PCBM structured films before and after treatment.....	44
Figure 16. FT-IR Transmission Spectra of non-treated and treated PCBM films...	46
Figure 17. XRD patterns of non-treated and treated glass/ITO/ PEDOT:PSS /CH ₃ NH ₃ PbI ₃ /PCBM structured films immersed in water.....	48
Figure 18. Absorption spectra of glass/ ITO/PEDOT:PSS/ CH ₃ NH ₃ PbI ₃ / PCBM structure for different concentrations of Stearic acid.....	50
Figure 19. Absorption Spectra of glass/ ITO/PEDOT:PSS/ CH ₃ NH ₃ PbI ₃ /PCBM for different Ethylenediamine concentrations.....	51
Figure 20. Device performance for varying concentrations of Stearic acid with (0.06 %) Ethylenediamine in IPA solution.....	54
Figure 21. Device performance for different concentrations of Ethylenediamine	56
Figure 22. J-V characteristics for best performing treated device and non- treated devices.....	58
Figure 23. Forward and Reverse Scan for best performing treated device.....	59

Figure 24. Device efficiency with time for devices stored in dark and humid condition.....61

Figure 25. J-V curves of treated devices with and without exposure to dark and humid condition, 40% RH.....62

Figure 26. Changes in the photovoltaic parameters for non-treated and treated devices.....63



List of Tables

Table 1. Photovoltaic Performance of Perovskite Devices for Varying Stearic acid Concentration.....	55
Table 2. Photovoltaic Performance of Perovskite Devices for Varying Ethylenediamine Concentration.....	57



Improved Stability of Perovskite Solar Cells with a Surface Treated Electron Transport Layer

Pesi Mwitumwa Hangoma

Department of Physics, The Graduate School

Pukyong National University

Abstract

Perovskite devices have garnered a lot of attention due to their remarkable opto-electronic properties such as high absorption coefficient, high charge carrier mobility and lifetime and long charge- carrier diffusion length. Within a space of 10 years, their efficiencies have quickly risen from 3.8% to 22.1%. However perovskite devices are unstable when exposed to air therefore limiting their use in outdoor application. This effect is even more apparent in inverted planar heterojunction structured devices with a p-i-n layout, which

use poly (3,4-ethylenedioxythiophene)-poly (styrene sulfonate) PEDOT:PSS as a hole transport layer and [6,6]-phenyl-C61 -butyric acid methyl ester PCBM as an electron transport layer. Devices based on this structure are preferable because they are hysteresis free, low temperature processing and high device efficiency as well as potential for use in flexible devices. In this study, we determine the primary source of device failure in our devices and based on this concept, we develop a technique that enhances the device stability of P-I-N PSCs. By surface treatment of the PCBM layer with hydrophobic Stearic acid, we achieved increased moisture resistivity of PCBM. The treated surface of PCBM has improved hydrophobicity and consequently prevents water ingress in the perovskite layer longer compared to non-treated surfaces. Importantly, treated devices exhibited improved stability in their photovoltaic parameters compared to non-treated devices when exposed to an environment of relative humidity (RH) 40%.

Chapter 1. Introduction

1.1 Research Background

Earth's demand for energy –which is fueled by an increasing population as well as increased standard of living, has increased rather significantly. The primary source of energy, oil, coal and fossil fuels however are finite resources, and concern has risen on how the world can be less dependent on these dwindling resources. In addition, research has shown that use of these resources has contributed to global warming due to the greenhouse effect. Thus, efforts have turned to seeking clean and renewable sources energy to help mitigate the effects of man's heavy dependence on fossil fuels. Renewable energy has a much lower impact on the environment as well as investments in it are spent on materials, workmanship, and the building and maintaining of facilities rather than costly imports. To add on, it provides growing price competition in an uncertain market. Sources of renewable energy can also be domestic, as it is becoming more technically challenging and expensive to source out fossil fuels, which are concentrated in certain regions, nations can import less and have diverse sources of energy thus increasing energy security.

Currently the main forms of renewable energy are wind, hydropower and solar energy-with tidal being developed. Of the three solar, energy is

advantageous in that energy from the sun provides a consistent and steady source of power throughout the year. To add on, solar cells are easy to maintain and are easy to install unlike geothermal and wind. In addition, they can be used in remote locations and although the initial cost is steep, there are zero recurring costs.

The past forms of solar cells have relied on silicon solar cells to harvest solar energy however the high cost of manufacturing, drives up the initial cost and is not feasible. Silicon solar cells, which are at the forefront of the technology, are reaching their practical limits and its getting hard to achieve higher efficiencies.

With this concern in mind, attention has turned to thin film photovoltaics an emerging technology that holds so much potential because of its versatility, their flexibility is advantageous for roll-to-roll processing resulting in cheaper manufacturing costs. In this field, perovskite solar devices are of particular interest due to their superb photovoltaic performance. Their excellent photovoltaic properties are because low exciton binding energy,^{[1][2]} ^[3,4] high charge carrier mobility and lifetime and its long charge carrier diffusion length ^[5,6] ^[7-9] and are thus being hailed as a promising next generation photovoltaic technology. In just a few years, their power conversions efficiencies have risen since the pioneering work of Miyaska, from 3.8%^[1] to 22.1%.^[10] Currently, conventional device structures are of two types, mesoporous and planar

heterojunction with either p-i-n or n-i-p layout which are fabricated using various methods such as one step method,^[11] two step method,^[12] blade coating and vapor deposition.^[13]

The problem though of their poor stability especially due to air exposure, is a hindrance to their commercialization and prevent them from being a viable option for outdoor photovoltaic activity. Of the many different structured devices, planar heterojunction p-i-n structured devices especially those based on a PCBM electron-transporting layer (ETL) with an Aluminum electrode as a back contact show poor stability. The reasons being, unlike other devices whose transport layers serve as some barrier to moisture thus slowing down perovskite degradation, PCBM being a small molecule does not provide full coverage of the perovskite film. It forms strong chemical bonds with H₂O and oxygen,^[14] also the usual film thickness of PCBM compared with other transport layers such Spiro-OMeTAD makes it a rather ineffective barrier against moisture and oxygen.^[15] With this in mind, alternative ETLs and electrodes have been sought as potential replacements for efficient and stable devices. Nonetheless p-i-n structures based on PCBM as an electron transport layer are still of particular interest because they are a low temperature processed^[16] which is beneficial for cheap manufacturing process, the J-V curves are free from hysteresis,^[17,18] as well as they are much easier to fabricate than other device structure. Also high electron mobility, energy level

matching and defect passivation are properties that makes its use more favorable than other ETLs.^[17] Aluminum as an electrode though unstable in air^[19] is equally favorable because of its low work function and is cheap compared to other metal electrodes.

In this study, PCBM was treated with Stearic acid through the use of a ligand Ethylenediamine, to improve its hydrophobicity^[20] and in turn, improve the stability of the device. After treatment, the surface had a larger contact angle and showed better moisture resistance when immersed in water compared to non-treated devices. Furthermore, treated devices could be stored for a longer time in air compared to Non-treated devices, for instance, treated PCBM devices retained most of their efficiency after exposure to air for within 2 hours compared to untreated devices, which maintained only 16% of their original efficiency. The best performing device had an efficiency of 15.28%, with a Voc of 1.01V, a Jsc of 20.82 (mA/cm²) and a fill factor of 0.72% against a non-treated device of efficiency 16.09%, Voc 1.00V, a Jsc of 21.92 (mA/cm²) and a fill factor of 0.73%.

1.2 Perovskite Structure

Gustav Rose discovered the original perovskite material CaTiO_3 in 1839. It is the name of a large family of oxide compounds with the general formula ABX_3 , which have a crystal structure related to CaTiO_3 . Generally, the perovskite crystal is usually inorganic but the material used in solar cells is a mixture of inorganic and organic compounds. The ideal crystal structure of the cubic ABX_3 as shown in Figure 1, can be described as having a number of corner sharing $[\text{BX}_6]$ octahedra with 'A' cation occupying the middle of the cube of eight surrounding octahedra.^[21,22] The more common mineral perovskite is slightly distorted and it is this distortion that is important for their magnetic and electrical properties.^[23] Structural work on perovskites was first carried out by Goldschmidt et al in the 1920's and it is from this work that the Goldschmidt tolerance factor (T) was derived. The tolerance factor is used to assess geometric stability and distortion of crystal structures in terms of the constituent ionic packing. T is defined by ratios of ionic radii A, B and X as $T = (R_A + R_X) / \sqrt{2} (R_B + R_X)$, where R_A , R_B and R_X are the ionic radii of A, B and X, respectively. ^[21,24,25] A value of $T=1$ indicates that the perovskite compounds has a cubic close packed structure. If the ratio of the ionic radii is different from the ideal value ($T \neq 1$), geometric strains and crystal distortions will surface. Thus, by calculating T , the crystalline structure of the perovskite can be predicted and its geometric strain and stability

evaluated. At the same time, T can be used to estimate the compatibility of different ions with a crystalline structure.



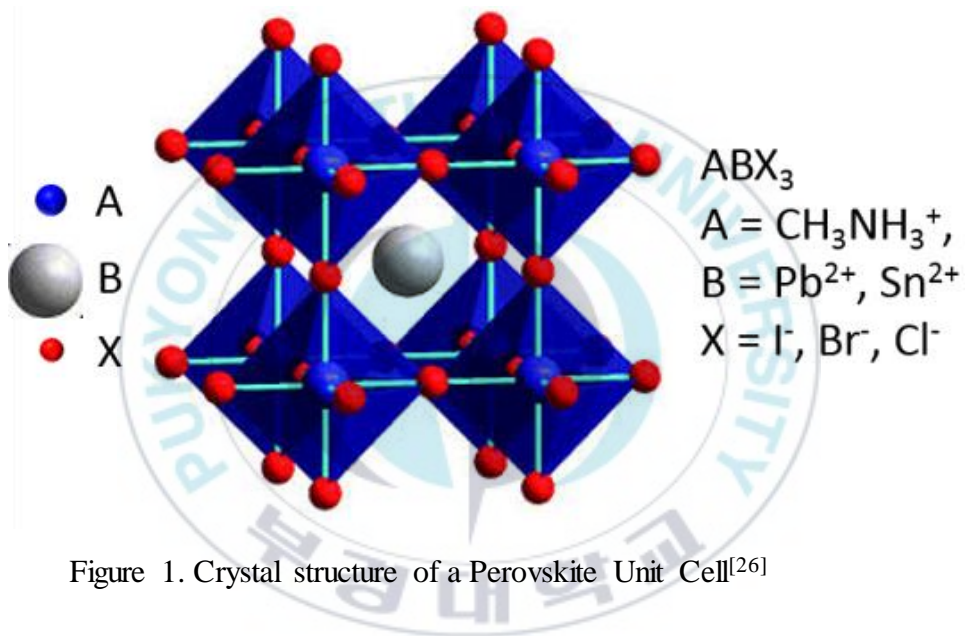


Figure 1. Crystal structure of a Perovskite Unit Cell^[26]



Figure 2. Increase in the power conversion efficiency of perovskite solar cells compared to other types of photovoltaics. Image: *National Renewable Energy Laboratory*

1.3 Working Mechanism of a p-i-n layered Planar Perovskite Solar Cell

The p-i-n structured device used in this study is shown in Figure 3. It is composed of two electrodes-the anode and cathode, an active layer, a hole-transporting layer and electron-transporting layer. The Indium Tin Oxide (ITO) surface works as an Anode and collects the positive charge whereas PEDOT:PSS is the hole transporting layer, the perovskite film serves as the active layer of the device, with PCBM as an electron transport layer, this is then made complete with the cathode such as a thin Aluminum layer which collects the electrons.

When the solar cell is exposed to light-in this case the solar simulator, the light strikes the active layer. The electrons then absorb photons with energy larger than the binding energy causing them to move to unoccupied states above the band gap, this in turn creates excitons. The built in potential generated by the different work functions of the electrodes causes the excitons to diffuse to an active layer/transport layer interface where they are separated creating free charges. These free charges are then collected at their respective electrodes. When an external field is applied, the charges travel to opposite ends creating a current and thus process is repeated.

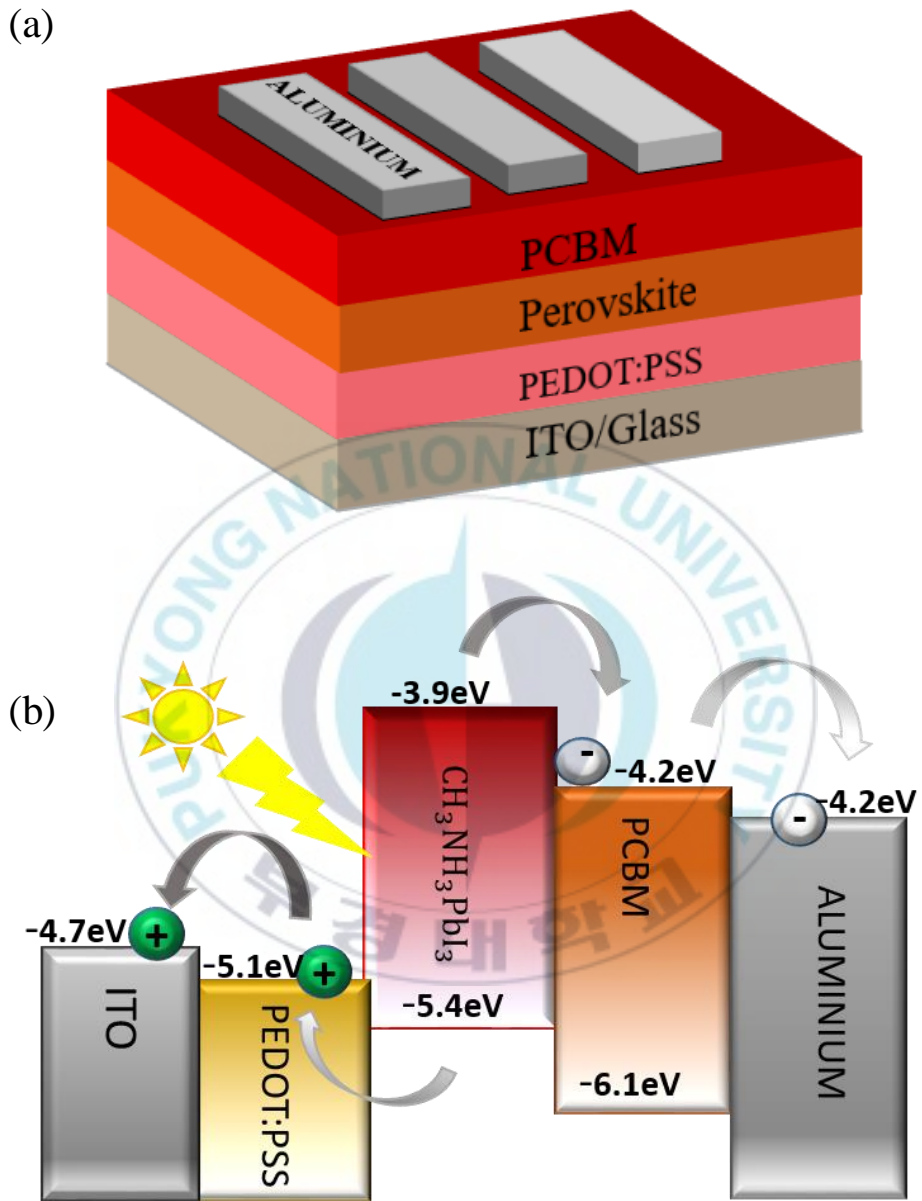
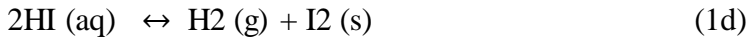
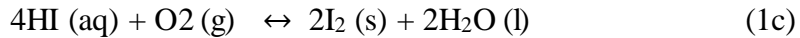
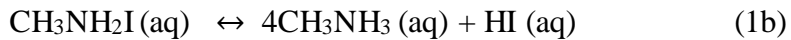


Figure 3. Device Architecture of a) planar heterojunction p-i-n layered device and b) mechanism of perovskite solar cell device.

Origins of Degradation

Investigations thus far have shown that degradation in devices is as result of heat, electric field, irradiation, intrinsic instability, moisture and oxygen and device architecture and components.^[27–29] However, the biggest cause of device degradation is moisture. When perovskite film devices are exposed to moisture, their characteristic reddish brown colour changes to yellow.^[30] So far, researchers have proposed various degradation mechanisms for the perovskite solar cell for instance, early on Niu et al suggested a degradation pathway based on the hydrophilic nature of the $\text{CH}_3\text{NH}_3^+(\text{MA}^+)$ cation. First H_2O diffuses through the PCBM film and hydrolyses $\text{CH}_3\text{NH}_3\text{PbI}_3$ (MAPbI_3) which degrades to $\text{CH}_3\text{NH}_3\text{I}$ (MAI) and PbI_2 . MAI further breaks down into (MA) and HI forms other products after reaction with oxygen. This is shown below;



Frost et al^[31] based their degradation mechanism on the basis that the interaction between water and perovskite is a Lewis base and acid interaction, where water is considered a Lewis base and the perovskite an acid. An

intermediate $[(\text{CH}_3\text{NH}_3^+)_{n-1}(\text{CH}_3\text{NH}_2)_n \text{PbI}_3] [\text{H}_3\text{O}]$ is formed when H_2O combines with $\text{CH}_3\text{NH}_3\text{PbI}_3$. Next, the intermediate finally decomposed into the products CH_3NH_2 , HI and PbI_2 . Leguy et al suggested that the 3D perovskite forms an intermediate hydrate after absorbing one molecule of water and then breaks into a non-dimensional structure (dihydrate perovskite) after absorbing another molecule of water and further irreversibly into final products.^[32] Dynamic simulations were carried out by Mosconi et al who showed to atomic level, the interactions between the surface of the perovskite film and water molecule among other findings, that water incorporated in the bulk crystal did not change the tetragonal structure of the perovskite.^[33] Yang et al suggested that the strong adsorption of water on the surface is due to the interactions of the electrons in the HOMO of the water with the unoccupied (CBM) of the MA cation surface.^[34]

Device components such as electrodes and electron transport layers as well, influence the stability of the device. Organic transport layers such as PEDOT:PSS are hydrophilic and being an acid, corrodes the ITO electrode causing further degradation.^[35] Studies were conducted to determine the effect of oxygen and water on PCBM, results showed a downward shift in the work function of PCBM when exposed to Oxygen and a downward shift in the ionization potential and work function of the film when exposed to water vapor, which was not recovered even with heating in vacuum. This shows that

there is a strong chemical interaction between PCBM and water molecules.^[14] In addition fullerene derivatives such C₆₀ and PCBM have a strong preference for metal interfaces due to their high surface energy^{[36][37]} and also charge transfers at this interface exist resulting in fullerene/metallic salts.^[38-40]

Another important feature of the PCBM and metal interface is that evaporated electrodes such as Gold, Aluminum, Calcium and Silver are able to penetrate fullerene layer.^[41,42] This results in a decreased electrical thickness of the layer and in turn the device stability.

Interaction between the perovskite film and electrode has been found to have negative effects on the device. Evidence of PbI₂ and AgI were found on Silver electrodes exposed to humidity of 50% and higher temperature in a study done by Kato et al showing that silver electrodes interacted with iodide forming silver iodide from silver oxide.^[43]

Guerrero et al investigated the degradation of devices in inert atmosphere and suggested a degradation mechanism without water as a trigger, thus hypothesizing that the S-shaped degradation of the device was associated with chemical degradation of the metal contacts due to their interaction with ions.^[44] This in turn creates irreversible degradation at the interface and consequently device instability.

1.5 Development in Device Stability

To solve the problem of instability due to the intrinsic material, researchers have suggested the use of 2 Dimensional perovskites as a solution as well as bilayer or multidimensional perovskites.^{[45][46,47]} 2Dimensional perovskites prevent penetration of water due to their dense compact layers, in addition, ion migration is suppressed thus increasing their lifetime compared to 3Dimensional perovskites. Based on degradation mechanisms due to moisture, researchers have made use of highly stable and water resistant materials to prevent ingress of moisture and oxygen and have yielded devices that are stable for up to 90 days. For instance, P3HT/SWNTs were used by Snaith et al as hole transporting layers with an extra layer, Poly(methyl methacrylate) PMMA, resulting in the device being protected from water ingress.^[18] Recently Alkylphosphonic acid ω -ammonium, polyethylene glycol, hydrophobic bulky alkyl ammonium cations and flouroalkylsilane groups have been assembled in the bulk or on the surface of perovskite film as a moisture-resisting layer yielding device efficiency in the range 12%~16.0% with device lifetime of 3months.^[34,48-50]

Thin tunneling insulating layers were also used as water barriers between the perovskite film surface and ETL resulting in water resistant devices with an efficiency of 19.2%.^[51] Also, Gratzel et al observed improved stability by using a dash of hydrophobic PMMA in the perovskite precursor solution

yielding and efficiency of 21%.^[52] Oxides such MoO_x , TiO_x , Al_2O_3 have been used as a buffer layer in the perovskite device for example Wang et al used Al_2O_3 in the device which saw it maintain at least 48% of its efficiency after being exposed to high humid conditions. Al_2O_3 was recently used on top of Spiro-OMeTAD by Atomic Layer Deposition giving it extra stability for a period of 24 hours.^[53] Yang Yang's group sought the use of non-organic transport layers based on the observation that use of organic layers e.g. PEDOT:PSS and PCBM resulted in quick degradation due to their low energies of formation.^[10] Their use of NiO_x and ZnO as HTL and ETL respectively gave their devices a stability of 90 days with an efficiency of 14.5%.^[35] MoO_x was used as buffer layer between Spiro-OMeTAD and an Aluminum electrode and reduced degradation in the device by preventing photo bleaching and formed a oxide layer which has protective properties thus increasing the stability of the device.^[54]

To increase the lifetime of devices with fullerene based ETL, moisture resistant organic buffer layers have been added between PCBM and the electrode, such as a thiol-functionalized cationic surfactant.^[22] Bai et al used a cross-linked silane-functionalized and doped fullerene to enhance the perovskite device performance and stability, which resulted in the device retaining most of their efficiencies after exposure to 30 days of air.^[24]

CHAPTER 2. Influence of Electrodes on Device Stability

2.1. Device degradation due to Aluminium Electrodes

To determine the influence of electrodes on the degradation of perovskite solar cells, the performance of the conventional device was examined by measuring their power conversion efficiencies (PCE's) after being exposed to air for a fixed time period. The devices were placed in a dark environment with 40% RH to rule out any instability from illumination. From Figure 4, the measured PCE's of devices fell rapidly from an original value of 16.15% to 2.69% at the 75th minute. From visual observation, there were no indicators of degradation in the crystal such as changes in color or corrosion in the active area of the device as observed in other studies.^[30,54] Mechanical damage in the electrodes was factored out by recording efficiencies for devices left in a glovebox for the same time length.

J-V slopes of the devices were also characterized as shown in Figure 5. The sigmoidal J-V slope of the exposed device is a characteristic feature of poor fill factor in devices. Poor fill factor is associated with increased defect sites, which induce charge recombinations and trap charge carriers at interface or bulk of the material which then cause irreversible degradation in the device. It is also linked with chemical degradation of the metal contact.^[44] However such slope is accompanied with a low J_{sc} and V_{oc} the slope in Figure 5

interestingly has no loss in V_{oc} and relatively good J_{sc} which does not correspond with the fill factor. This implies that the problem might not lie with the bulk of the material but merely at the interface.



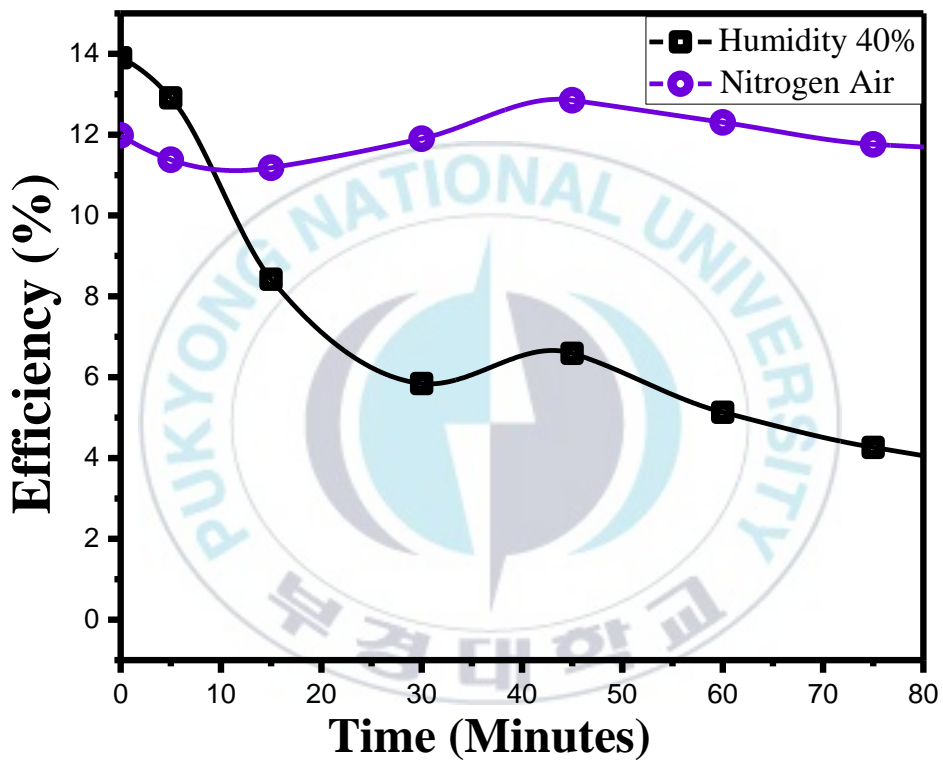


Figure 4. Device efficiencies with time for samples stored in a humid level of 40% and Nitrogen gas.

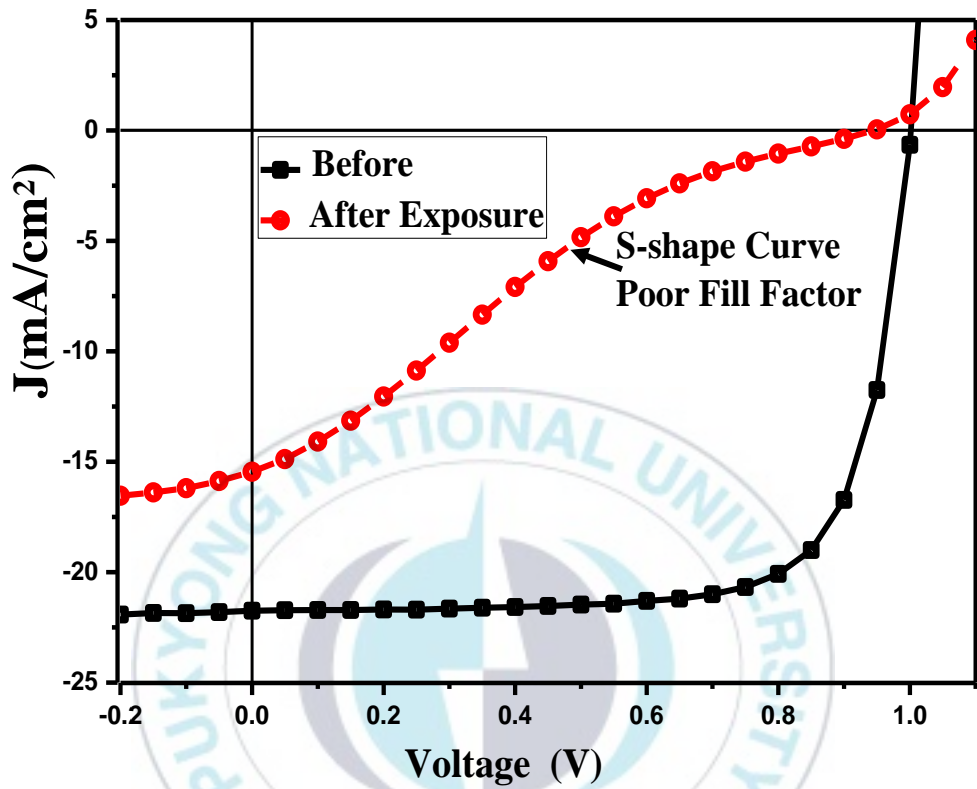


Figure 5. J-V curve of the original device, device exposed to air and a device with redeposited electrodes. Note the sigmoidal curve associated with chemical degradation at the Electrode interface of the device.

2.2 Surface Observation of the Exposed Film

Placing the film under the microscope, changes on the surface of the film were observed after exposing the device to a humid environment with a level of 40% for 1 hour. From Figure 6a, the film surface of the pristine device has a clear surface on the electrode, however, after exposure the black spots seemed to appear which increased and in number when the device was exposed in air for longer and further changed to white spots as observed in Figure 6c. This change indicated that some chemical reaction was present between the organic layers and the electrode. To rule out present solvents as a factor, the devices were thermally annealed for 60 minutes, Figure 6b, as opposed to 10 minutes for the conventional device, however the surface showed similar changes as the rest of the devices as shown in Figure 6d.

A sample placed in nitrogen condition overnight, Figure 6b however did not show similar conditions and maintained the smooth surface, which was observed in the original sample, which corresponds to their constant efficiencies when measurements were carried out in the glovebox. It is well known that Aluminum is not the first choice of an electrode due to its tendency to oxidize in air,^[19] however Aluminum films exposed in air did not show the same surface changes as shown in samples with same condition. Therefore, the surface change could not lie solely on air but as a result of the interaction between the perovskite and electrode.

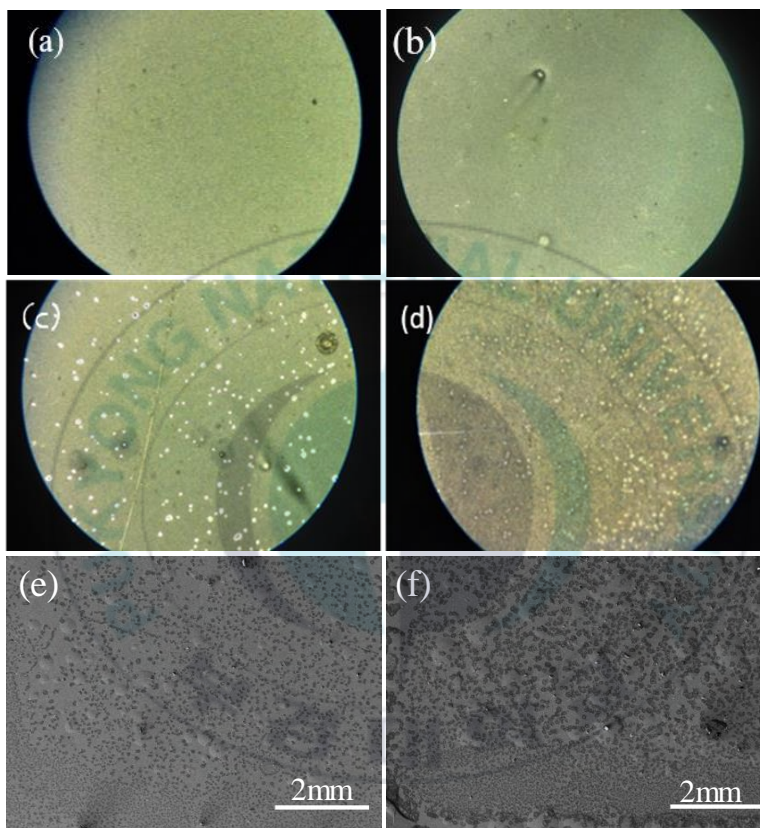


Figure 6. Optical microscope images of the Aluminum electrode surface 4X magnification for a) device without exposure to humidity and b) device left overnight in Nitrogen gas. c) Device exposed to humidity at 40% RH, and d) device thermally annealed for 1 hour. e) and f) show the top-view SEM images of the device before and after exposure to humid condition.

2.3 X-Ray Diffraction

To determine the source of the drop in efficiency, we performed X-Ray Diffraction (XRD) on the bulk structure. The X-Ray Diffraction patterns shown in Figure 7 indicate that the crystal structure of the exposed device was still intact at 75th minute. The major peaks identified corresponded to the (110) and (220) crystal planes of the MAPbI₃ perovskite tetragonal structure.^[55] The tetragonal structure is present in the perovskite when it is in a hydrate state.^[32] Comparing the two patterns, the intensity of the peaks for films exposed to the surface were less than that of the films in the initial condition, which has been explained to be as a result of change in domain size. For the exposed device, no additional peaks corresponding to PbI₂^[49] which is a characteristic of a hydrolyzed perovskite film. A film with this quality is expected to yield efficiency values similar or slightly lower to that of a pristine device and is not consistent with the low efficiency obtained from the devices. This result raises further questions on the primary source of device instability in our devices.

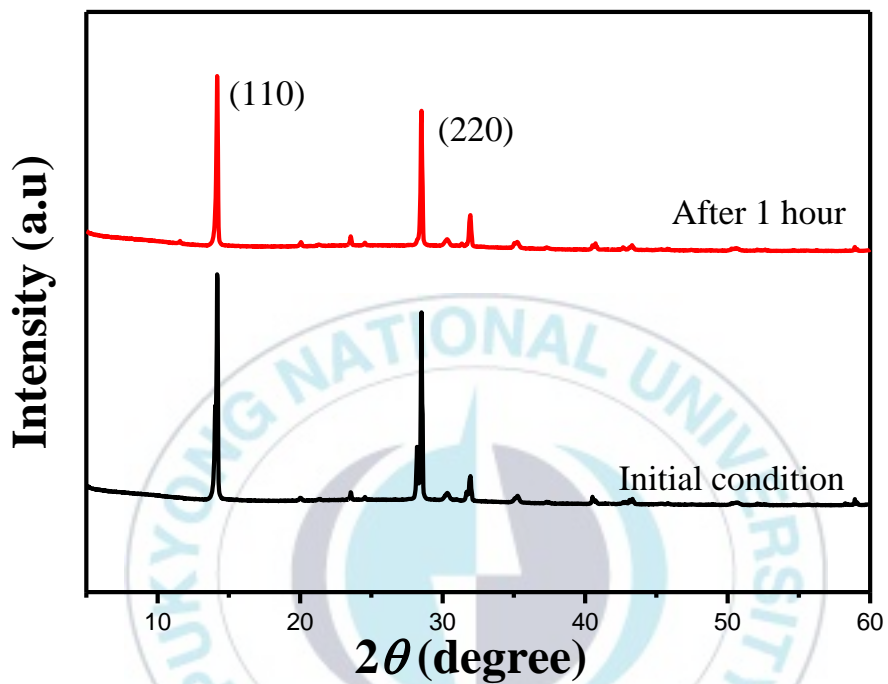


Figure 7. XRD patterns of glass/ITO/PEDOT:PSS/CH₃NH₃PbI₃/PCBM structured films covered by Aluminum electrodes exposed to air vs films stored in Nitrogen gas.

2.4 Electrode-Influenced Degradation Mechanism

We suggest a mechanism that explains the drop in device efficiency based on the chemical degradation of the electrode catalyzed by the presence of H₂O and Oxygen. The reaction leads to Aluminium Iodide, AlI₃, being formed at the PCBM/Al interface, which gives the S-shaped characteristic similar to that of Guerrero et al.^[44] The mechanism is similar to that of Kato et al for silver atoms under humid conditions.^[43]

H₂O molecules penetrate the surface of PCBM and diffuses into the perovskite film, which forms a hydrate and starts to degrade into MAI/HI. HI then diffuses through the perovskite film and penetrates the PCBM to react with the metal electrodes forming an insulating layer of AlI₃. As time is increased, this process is accelerated and the layer of AlI₃ increases which negatively affects the fill factor and corresponds to a drop in efficiency depicted in Figures 3 and 4. The illustration of this mechanism is shown in Figure 8. This reaction builds up until the perovskite film is completely decomposed as indicated by the color change, until the device is unable to function.

These ions could in turn react further with the Aluminum giving a result similar to that of a previous report on Ag.^[43] If we remove the Aluminum film, we indirectly remove this insulating AlI₃ film, which in turn reduces the defect sites and trapped charges and thus improves the surface fill factor that should

be reflected by a change in the J-V slope. When the electrodes were redeposited, the original J-V slope was obtained albeit with a smaller fill factor compared with the original. Nonetheless the restored J-V slope indicated that the poor fill factor in the exposed device was mainly due to degradation of the metal contact at the PCBM/Al interface as shown by previous reports.^{[[40,42]} Also the device efficiency with time is observed for devices with multiple electrode redepositions, shown in Figure 9b, versus devices without any redeposition. After redeposition, the devices had approximately 80% of their efficiency restored, which gave a more accurate picture of the ability of the device to function. Figure 9b shows that replacing the electrodes after certain intervals increased the lifetimes of the devices due to the limited time of interaction between the active layer and electrodes.

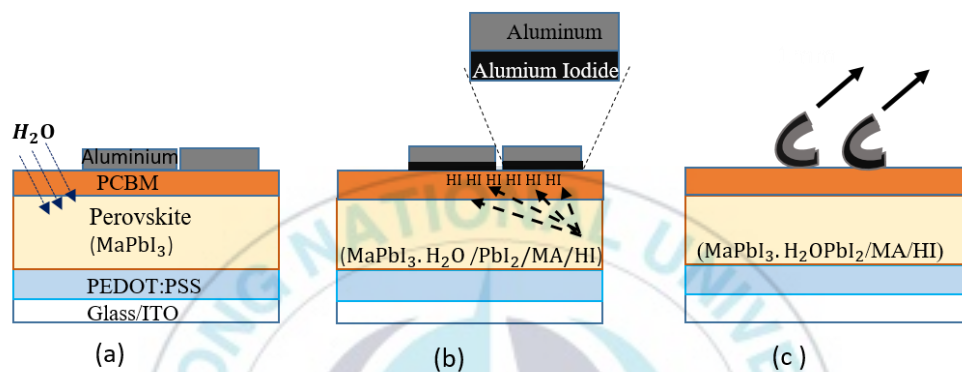


Figure 8. An illustration of the formation and removal of AlI_3 from the perovskite device. At a) H_2O penetrates the PCBM film and diffuses through to the perovskite film. b) Due to the hydrophilic nature of the MA cation, an intermediate hydrate phase is formed and further breaks down to form HI and other ions, which migrate to the surface of the device. This forms an AlI_3 film due to the strong interaction between Al and HI and causes poor device performance. Removing the electrodes at c) removes this film and restores the pristine surface.

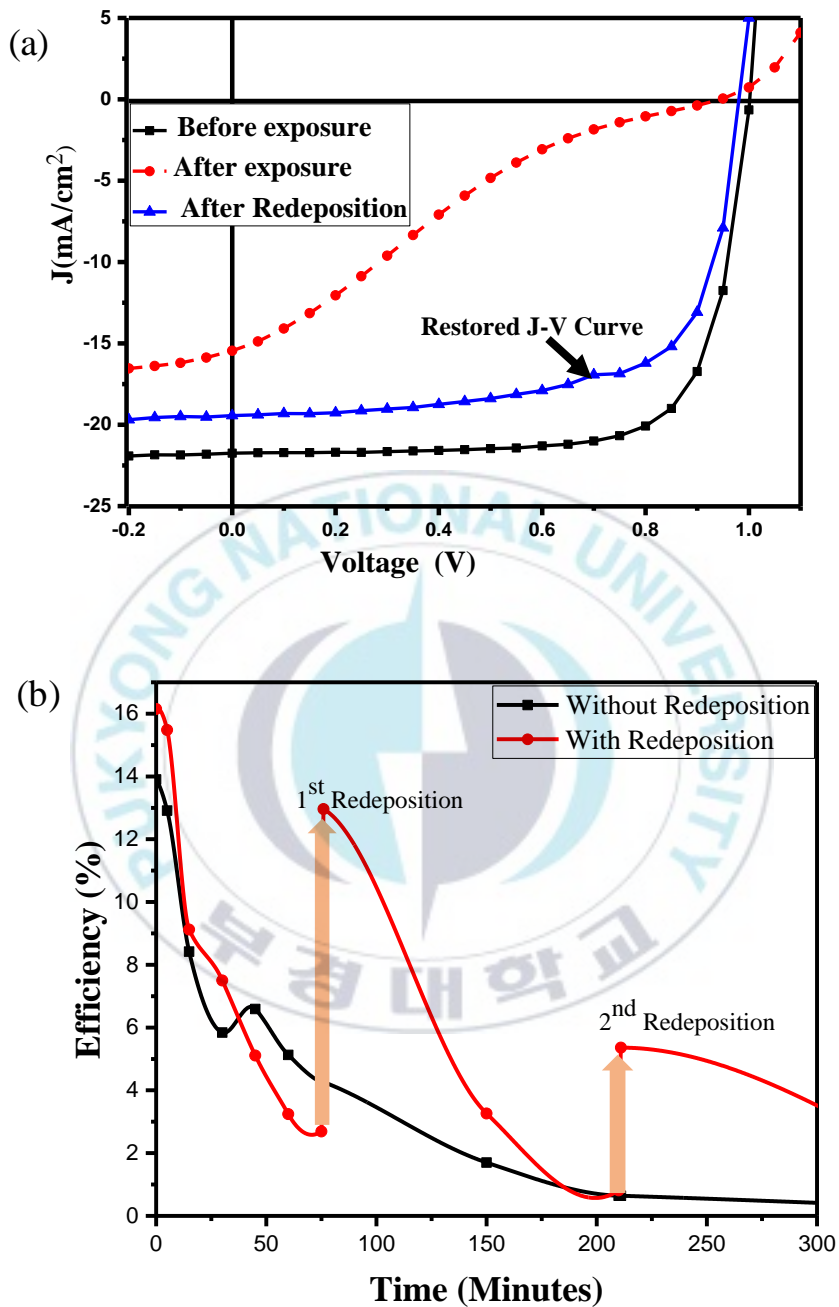


Figure 9. J-V characteristics of devices with a) a redeposited electrodes after exposure to humidity. b) Efficiencies of devices with time for samples with and without electrode redepositon

Chapter 3. Surface Treatment of the Electron Transport Layer

3.1 Stearic Acid and Its Applications

Having established a cause for the device instability within the first hour or so of storage in humid conditions, we considered using materials that could prevent moisture from penetrating the active layer and in turn prevent further reactions with the electrode. This would consequently improve the stability of the device. Stearic acid was selected as suitable material to use in the device.

Stearic acid also known as Octadecanoic acid, is a fatty acid composed of 17 hydrocarbons in a linear chain and a carboxylic (COOH) group as shown in Figure 10a. The acid has been used on various surface such metals, metal oxides, PMMA, calcium and even bentonite to make them super hydrophobic by self-assembled closely packed monolayers.^[20,56,57]

The manner in which Stearic acid is chemically adsorbed on the surface has been studied using the Langmuir procedure. The acid anchors on the polar surface through the hydrophilic carboxylate group and the hydrophobic hydrocarbon tail perpendicular to the surface.^[57] The growth of closely packed self-assembled monolayers on a substrate which is usually done using the Langmuir-Blodgett technique.^[58] The technique involves adsorbing one or more layers of an organic material by dipping the substrate in a liquid

containing the organic material. The assembly and growth and packing of these monolayers are influenced by various factors such as the head of the acid and the substrate surface as well solvent temperature, concentration, growth time, degree of surface dehydration, and contamination of the substrate itself.^[56,59] That being said, the exact nature in which the acid monolayers attaches to each substrate is unique and its orientation characteristics are observed using ellipsometry.



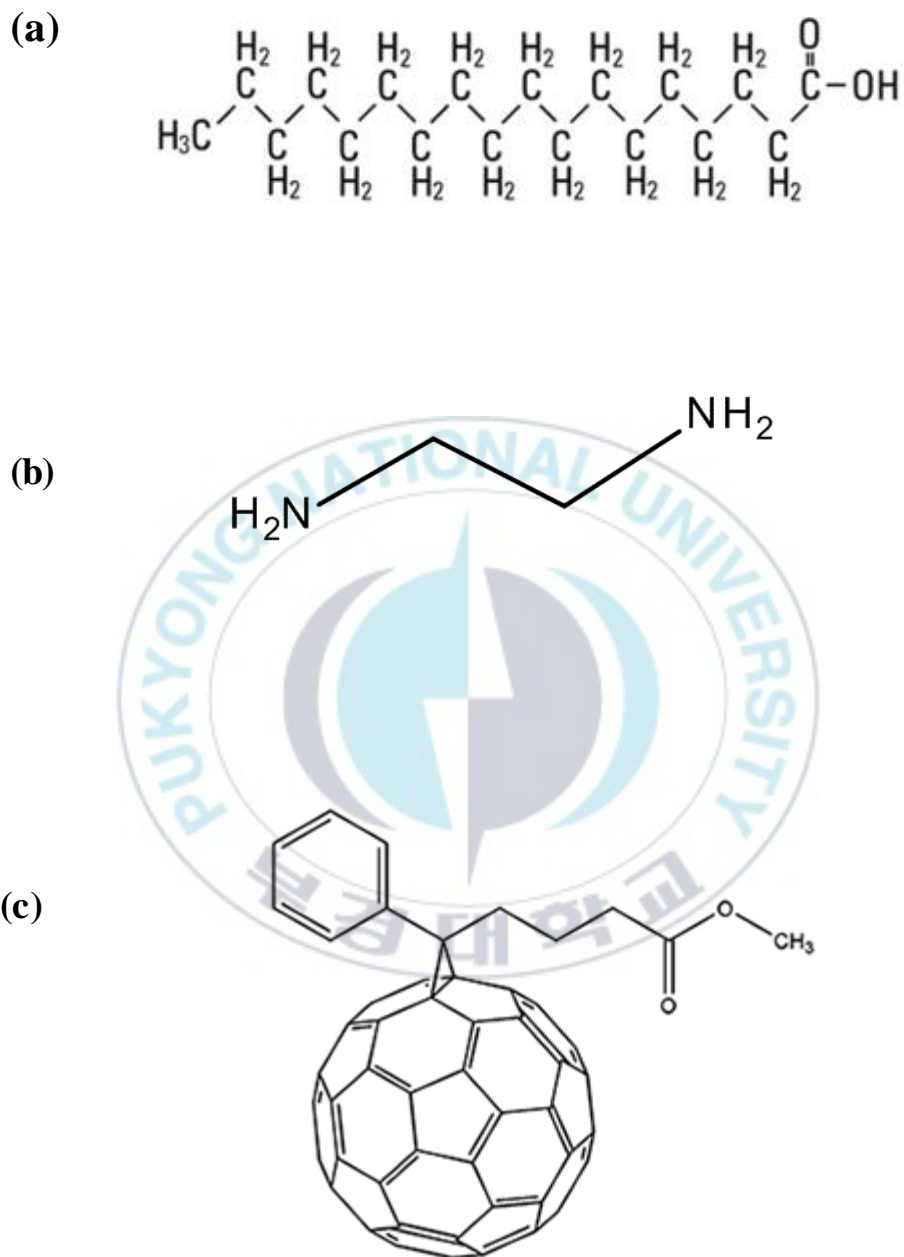


Figure 10. Chemical structure of a) Stearic Acid b) Ethylenediamine and c) PCBM.

3.2 Device Fabrication

Materials preparation: All reagents purchased from Sigma-Aldrich were used without further purification. Methyl ammonium iodide (MAI) was synthesized as follows:

24 mL methylamine, 33wt% absolute ethanol, was reacted with 10mL hydroiodic acid (HI) 57wt% in water in a 100mL round bottom flask bottom flask under nitrogen at 0°C for 2 hours with stirring. Then, the reacted solution was dried by rotary evaporation at 50°C; a white powder of MAI was formed. For purifying the pristine MAI, dried MAI powder was dissolved in ethanol followed by sedimentation in diethyl ether by stirring the solution, this process was repeated three times and a high purity MAI powder was recovered and dried at 60°C in a vacuum oven for a period of 24 hours.

Device Fabrication: Thin-film perovskite solar cells were fabricated on an indium tin oxide (ITO)-coated glass substrate with the following structure; ITO coated glass substrate / poly (3,4-ethylenedioxythiophene)-poly (styrene sulfonate) (PEDOT:PSS)/CH₃NH₃PbI₃ active layer / [6,6]-Phenyl-C61 -Butyric acid Methyl Ester (PC₆₁BM)/Al. The ITO-coated glass substrate was first cleaned with detergent, ultra-sonicated in acetone and isopropyl alcohol, and subsequently dried overnight in an oven at 100°C. PEDOT:PSS (Baytron PH) was spin-casted on the ITO at 4500 rpm from aqueous solution to form a film of 40 nm thickness. The substrate was

dried for 10 min at 140°C in air and then transferred into a glovebox to spin-coated the perovskite active layer. A solution containing a mixture of MAI:PbI₂ with a molar ratio of 1:1 in DMF/DMSO solvent with concentration of 40wt% was then spin-coated first for 1000 rpm for 5 secs followed by 5000 rpm for 50s on top of the PEDOT:PSS layer. Chlorobenzene was the dropped after a 5-second delay. Afterwards, the PC₆₁BM (30 mg/mL in chlorobenzene) was deposited by spin coating at 1500 rpm for 30 s. The precursor perovskite film was dried in a vacuum oven by heating at 120°C for 10 minutes. Lastly, Aluminum (Al, 100 nm) electrode was deposited by thermal evaporation in a vacuum of about 5×10⁻⁷ Torr.

Stearic acid treatment: The active layer and transporting layers were coated as for conventional devices. After annealing, the devices were left to cool in the glovebox. They were then transferred in air and Ethylenediamine (2.4ul/mL in IPA) was spin coated on top of the PCBM film at 4500rpm for 60 sec. Next Stearic acid was coated by dipping the devices in IPA solution for 20 seconds at 50° C before being spin coated for 60 seconds at 4500 rpm. Lastly, Aluminum (Al, 100 nm) electrode was deposited by thermal evaporation in a vacuum of about 5×10⁻⁷ Torr.

Film Characterization: The UV-visible absorption spectra of perovskite film were recorded by a Varian 5E UV/VIS/NIR spectrophotometer. The XRD spectra of perovskite film were measured using an X'Pert-MPD (Philips,

Netherlands). The surface morphologies of perovskite film and electrode were obtained by scanning electron microscopy (SEM, S-2700, Hitachi, Japan) and an optical microscope. AFM was conducted to observe the change in the surface roughness before and after the treatment of PCBM on the perovskite films. FT-IR spectra was used to determine the chemical composition of the devices before and after modification of the PCBM layer using JNM ECP-400, JEOL (Japan).

Photovoltaic Characterization: Current density-voltage (J-V) characteristics of the devices were measured using a Keithley 236 Source Measure Unit. The performance of perovskite solar cells was measured by using an Air Mass 1.5 Global (AM 1.5 G) solar simulator with an irradiation intensity of 1000Wm^{-2} .

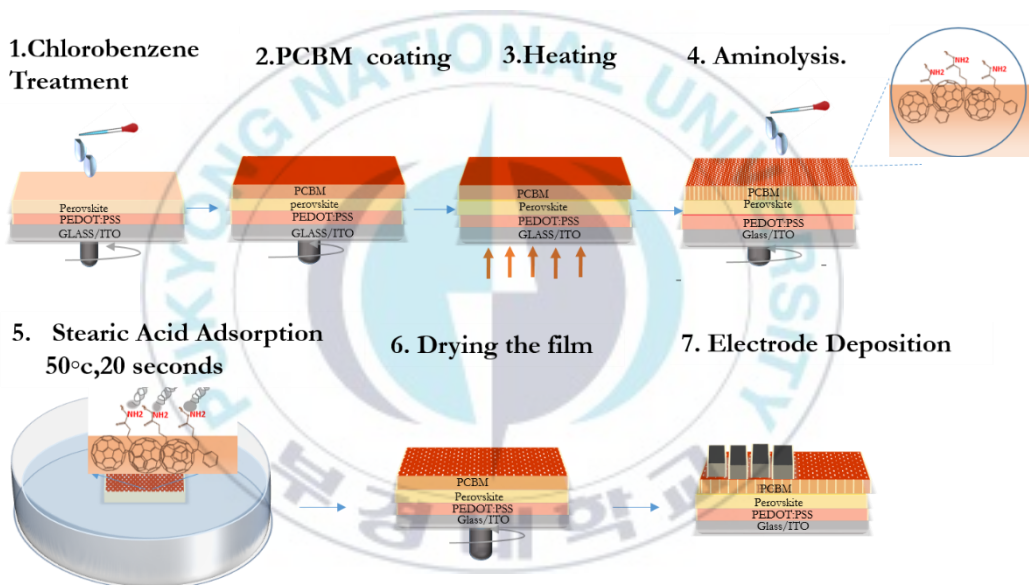


Figure 11. Schematic of the fabrication and adsorption of Stearic Acid on perovskite device with a glass/ITO/PEDOT:PSS/CH₃NH₃PbI₃/PCBM/Al structure.

3.3 Adsorption of Stearic Acid on the Surface of PCBM

The concept used to treat the surface was inspired by X.Lu et al who worked on a PMMA surface. Stearic acid through its alkyl chains, lowers the surface energy of the substrate and increases the contact angle making the surface hydrophobic, which is given by Young's equation,

$$\cos \theta = (\gamma_{sv} - \gamma_{sl})/\gamma_{lv} \quad (2)$$

where θ is the contact angle and γ_{sv} , γ_{sl} and γ_{lv} are the various surface tensions in the system.

Assembling the chains to create a rough surface on the substrate is more advantageous because increased roughness increases the degree of the contact angle and has been correlated using Cassie's and Wenzel's models, is described by the equation,^[34,60,61]

$$\cos \theta_r = r \cos \theta \quad (3)$$

θ and θ_r are the intrinsic contact angles for a smooth and rough surface respectively and r is the roughness factor.

To guide the assembly of the alkyl chains on the substrate, Ethylenediamine was used. Ethylenediamine whose chemical structure is shown in Figure 10b, is a strong basic amine and is used as a building block in chemical synthesis as well as to aminolyse various compounds. The group worked to control the growth of Stearic acid through aminolysis of the surface ester groups of the

substrate. Two factors were important in this preparation, the time of the aminolysis and the temperature of reaction between the Stearic acid and amide groups. The Ethylenediamine works by forming partial amide groups on the surface ester groups (-CO-NH₂) of PCBM.^[23] Thereafter, Stearic acid reacts with the amino groups through the carboxylic head group and the unreacted Stearic acid is induced to crystallization. The technique resulted in an already hydrophobic surface becoming superhydrophobic.

The structure of PCBM given in Figure 10c, which is a fullerene derivative, is composed of fullerenes and methyl ester groups, therefore it was speculated that the surface treatment could be applied on PCBM. Treatment was used after the perovskite was fabricated as illustrated in Figure 11, using the merged annealing process.^[30]

The surface of PCBM is functionalized firstly by spin coating Ethylenediamine in IPA solution on the film. The concentration of Ethylenediamine was optimized by varying its concentration in the IPA solution. Copious amounts of Ethylenediamine was detrimental to the PCBM surface, thus a small concentration was used to prevent negative effects on the substrate. Increasing the concentrations resulted in a color change of the device and increased pinholes; therefore, it was imperative that good film quality was a prerequisite to aminolysis. After aminolysis, the ITO glasses

were dipped in a Stearic acid-IPA solution at 50⁰C to allow the Stearic acid to react with the Ethylenediamine.

The concentration of the Stearic acid was optimized for the devices with increased concentrations resulted in a white film over the devices, which affected the electrodes deposited on them. The substrates were then dried by spin coating. Thereafter electrodes were deposited via thermal evaporation.



3.4 Water Resistivity of the Treated Surface

The contact angle of Glass/ITO/PEDOT:PSS/perovskite/PCBM structure was measured to assess whether the hydrophobicity of the functionalized PCBM film with moisture resisting features had improved.^[15, 34] The contact angle (CA) was determined by dropping 4ul of water on the surface of the treated and untreated device. From visual observation, the surface of the treated PCBM film had a contact angle of larger than 90° compared with the surface of the conventional device, which had a contact angle lower than 90°. This images of which can be seen in Figure 12a and Figure 12b which proved that the treatment was successful.

When both samples were immersed in water as seen in Figure 13(a-d), the non-treated films degraded at a faster rate compared to treated films. The non-treated device changes its color from brown to yellow, a visual indicator of decomposed perovskite at the 5 second mark whereas hardly no change is observed in a treated device, indicating that the hydrophobic surface works across the film of the device. XRD patterns were observed for the film of a non-treated and treated device.

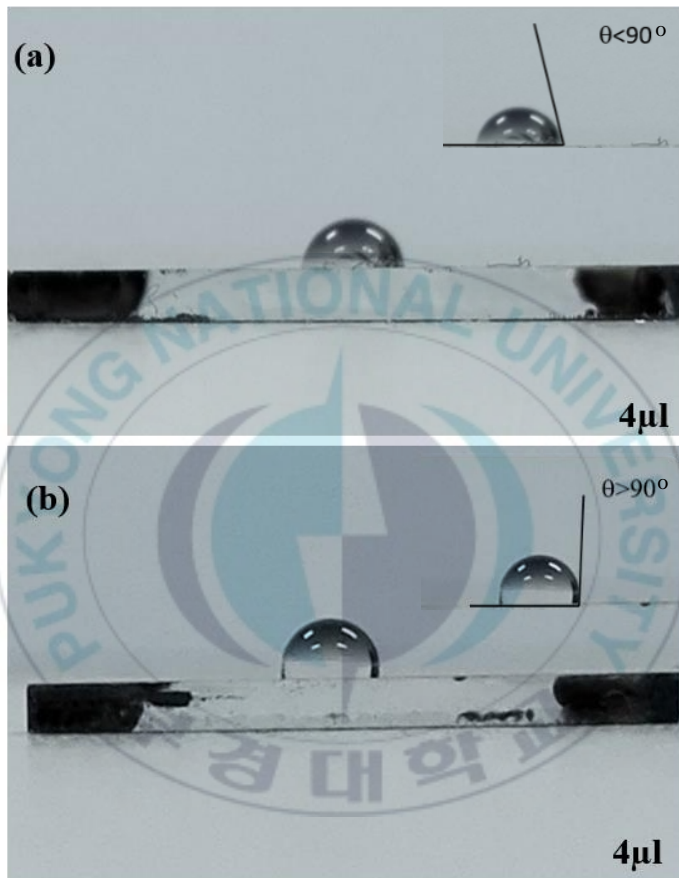


Figure 12. Contact angle for a) a non-treated film and b) treated film 6g/ml Stearic acid in IPA solution and (0.06%) Ethylenediamine. The measurement was done with 4 μl deionized water droplet.

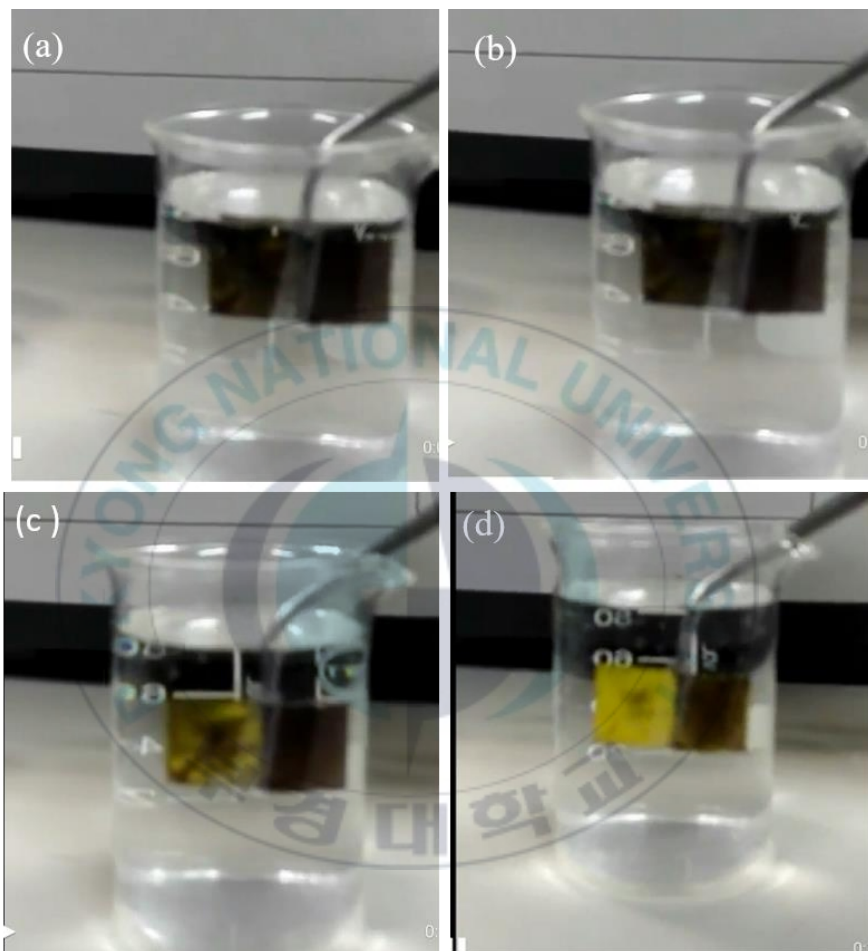


Figure 13. Water resistivity of non-treated and treated glass/ITO/ PEDOT:PSS / $\text{CH}_3\text{NH}_3\text{PbI}_3$ /PCBM structured films when immersed in room temperature water for a) initial b) 5 seconds c) 10 seconds and d) 19 seconds.

Chapter 4. Results

4.1 Scanning Electron Microscope

The film morphologies of Glass/ITO/PEDOT:PSS/perovskite/PCBM structured films were observed through top-view SEM in Figures 11(a-c). We can see the effect of aminolysing the surface using Ethylenediamine for constant concentration of (6g/ml in IPA) Stearic acid. Without using Ethylenediamine Figure 11b is as smooth as the pristine PCBM surface however, from Figure 12(d-f), we see the effect of temperature on the formation of the Stearic acid layer of the device. The concentration of the Stearic acid was increased for improved visual observation, as images for the optimized film thicknesses showed no significant difference. At room temperature, it was observed that flat surfaces of Stearic acid was formed. As the temperatures were increased, the round clusters were decreased and sharp jagged-like planes of stearic acid were formed which was the desirable morphology as referenced from X.Lu et al's work. The grains of the surface are visible through the Stearic acid layer indicating that though insulating, the layers are thin enough to allow efficient collection of electrons by the Aluminum electrode but are thick enough to reduce moisture and perhaps electrode penetration in the device.

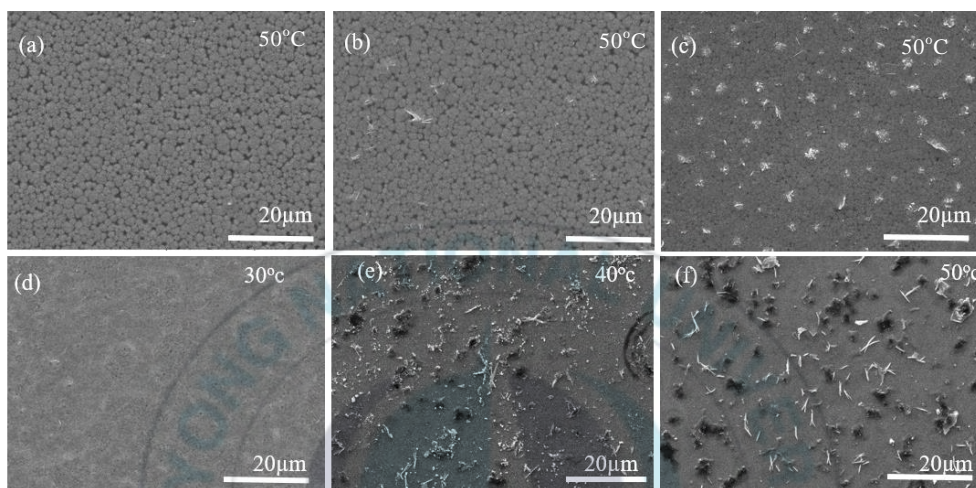


Figure 14. Top-view SEM images of the surface morphology of glass/ITO/PEDOT:PSS/CH₃NH₃PbI₃/PCBM structured films a) before treatment, b) after Stearic acid treatment and c) Stearic acid treatment after aminolysis. Effect of temperature on crystallization of the Stearic acid on the surface for a concentration of 10g/ml at d) 30°C e) 40°C and f) 50°C.

4.2 Atomic Force Microscopy

Three samples with a glass/ITO/PEDOT:PSS/CH₃NH₃PbI₃/PCBM structure were prepared and placed under the microscope. We observe from Figure 15a that though the overall surface of the film has some roughness due to the boundaries of the grain, the surface of the grains is smooth. This morphology explains the low contact angle observed in Figure 12a. In Figure 15b, the surface shows no change in its morphology after aminolysis except for little bumps due to chemical interaction with PCBM. However in Figure 15c it is evident that there is significant change in the surface texture after Stearic acid treatment. The surface roughness increases significantly along the grains of the film indicating that the method was successful in guiding the orientation of the CH₂ chains and crystals of Stearic acid. It is further observed that the pockets of air can be created with this morphology, which according to Wenzel's model, is required for an increase in contact angle.

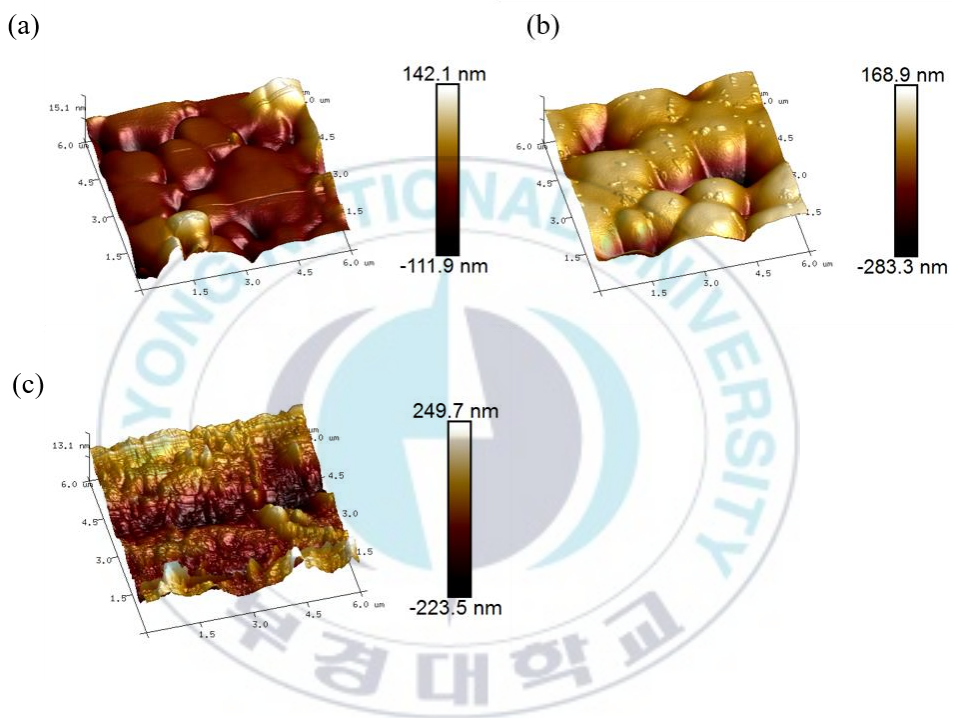


Figure 15. AFM of the surface topography of treated glass/ITO/ PEDOT:PSS /CH₃NH₃PbI₃/PCBM structured film a) before treatment, b) after aminolysis and c) Stearic acid treatment.

4.3 Fourier Transform Infrared Spectroscopy

Fourier Transform Infrared Spectroscopy Transmission Spectra of the Non-Treated and Treated films was carried out to confirm the formation of Amide linkages and (-COOH-) Stearic acid on the surface. The non-treated and treated films were prepared on ITO surfaces and scraped off. The powder was then collected and analyzed. The spectra before treatment was then compared with that of the reference literature^[20] to confirm the existence of the desired linkages. As can be seen from Figure 16, after treatment we confirm the presence of amide I ($\nu(\text{C}=\text{O})$) and amide II (N-H) at approximately 1660 cm^{-1} and 1550 cm^{-1} which indicates that Ethylenediamine did react with PCBM though partially as can be confirmed through the presence of the methyl ester band at approximately 1750 cm^{-1} before and after the reaction. After treatment with Stearic acid we see two peaks appear at approximately 2900 cm^{-1} and 2800 cm^{-1} which correspond to the asymmetric and symmetric stretching vibration of CH_2 chains of Stearic acid.^[62] This is an indication that Stearic acid did react with the surface amino groups as well as crystallized on the surface.

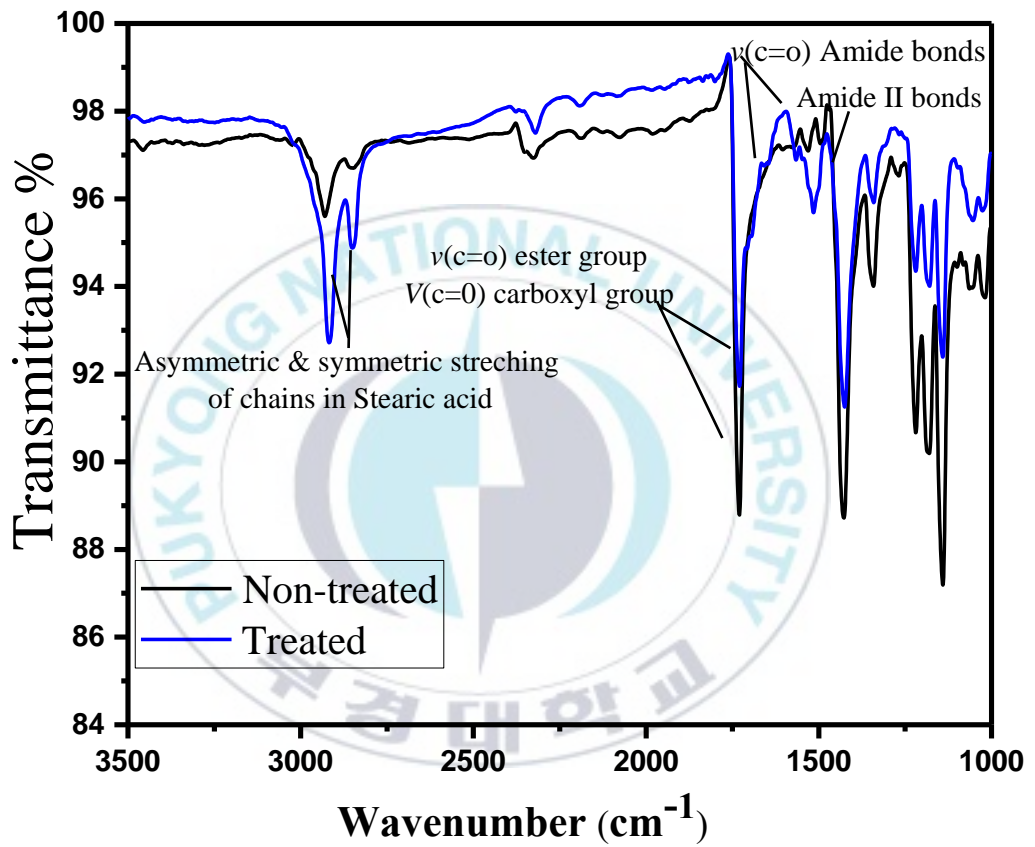


Figure 16. FT-IR Transmission Spectra of non-treated and treated PCBM films.

4.4 X-Ray Diffraction

X-Ray Diffraction of Glass/ITO/PEDOT:PSS/perovskite/PCBM structured samples was used to determine the crystallinity of perovskite films after Non-treated and treated samples were immersed in water as shown earlier in Figure 13. Dominant peaks characteristic to the perovskite crystal, (110) and (220) at 14.15° and 28.46° respectively in both Figure 17a and Figure 17b appear for samples before immersion in water referred to as the initial condition. These peaks decrease in intensity for increased time in water. For the untreated device, Figure 17a, the dominant peaks of the perovskite films at 10 seconds disappear indicating that the perovskite film is completely degraded. On the other hand, peaks characteristic of PbI_2 at 12.7° and 25.9° for (001) and (101) planes respectively begin to appear. These peaks increase in intensity for a longer soaking time from 10 seconds to 20 seconds as shown in Figure 17a. However, perovskite films with a treated PCBM surface showed delayed breakdown in the crystal structure of the perovskite, the dominant peak of PbI_2 in Figure 17b at 12.7° only appears at the 20-second mark in the presence of perovskite dominant peaks (110) and (220). This corresponds with the photo of the film in Figure 13d at 20 seconds. The film is still brown in color after 20 seconds in water.

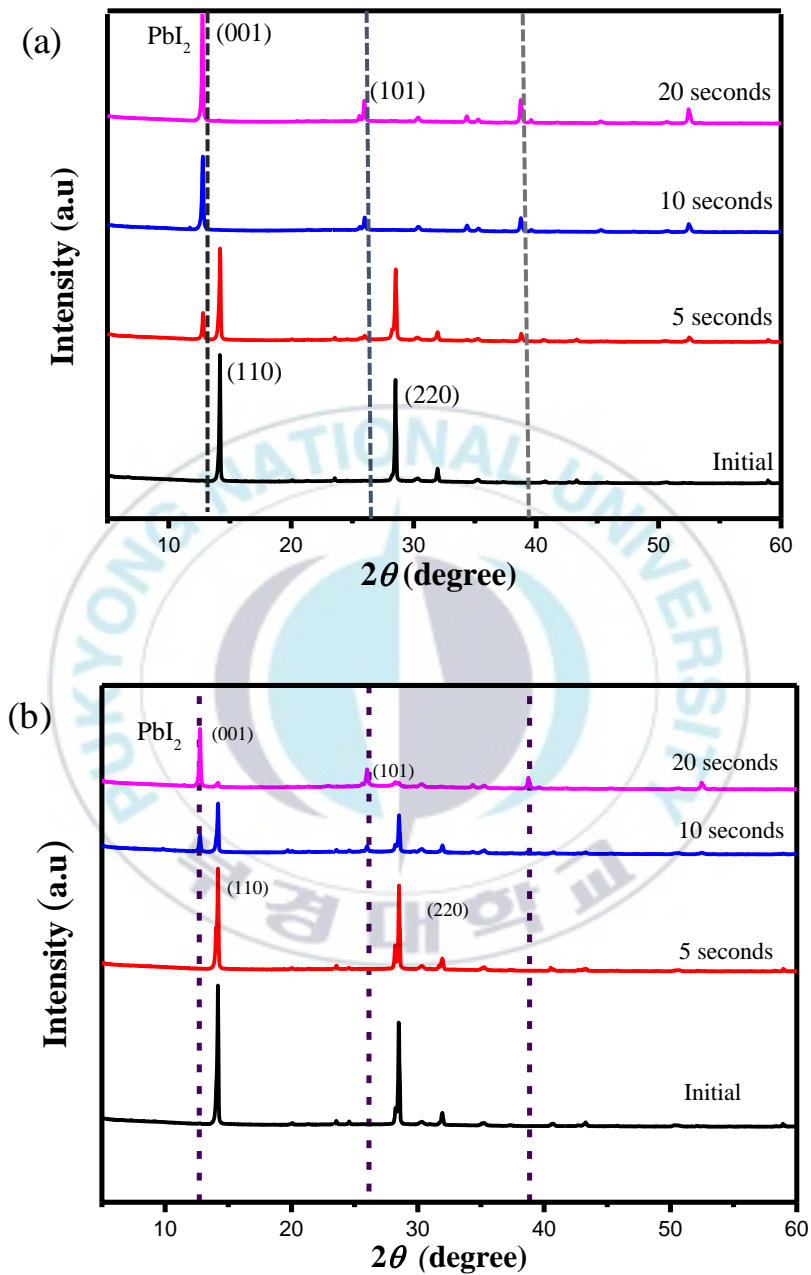


Figure 17. XRD patterns of a) a non-treated film and b) a Stearic acid-treated film immersed in water for different times. The peak associated with PbI_2 is more dominant in the non-treated device.

4.5 UV-visible Absorption

Figure 18 and Figure 19 show the absorption spectra of glass/ITO/PEDOT:PSS/perovskite/PCBM structured film for increasing concentrations of Stearic acid and Ethylenediamine respectively. For increasing concentrations 8g/ml and below, the trend of the spectra such as shape, absorption intensity and bandgaps were more or less consistent with the spectrum of the non-treated structure implying that for these concentrations, Stearic acid did not significantly alter the optical performance of the device. However, there was a significant shift in the absorption edge of the spectra between 700nm-800nm for concentrations 10g/ml and above. The shift towards the left could be ascribed to the reduced ratio between the upper layer and the perovskite film resulting in a composite absorption spectra of the perovskite film and Stearic acid spectra. When Ethylenediamine was increased, the trend and absorption of the spectra remained more or less. This lead to the conclusion that the amount of Ethylenediamine used in this study had no influence in the device optical properties indicating that the addition of Ethylenediamine and Stearic acid did not alter the optical properties of the active layer nor the transporting layers of the device.

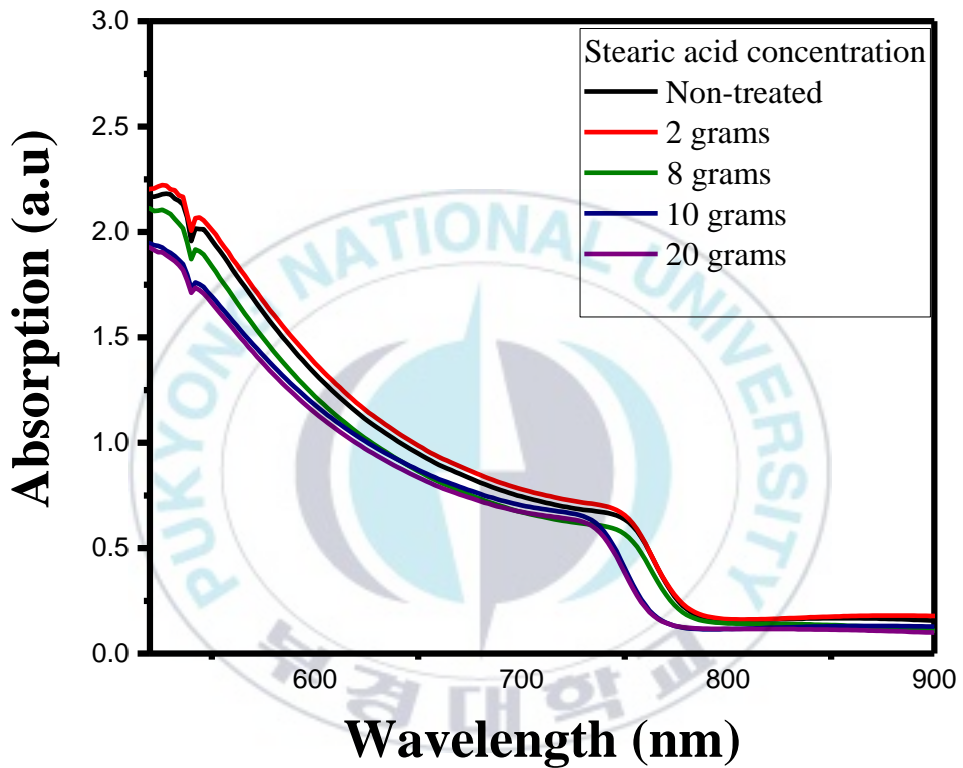


Figure 18. Absorption spectra of a Glass/ ITO/PEDOT:PSS/ $\text{CH}_3\text{NH}_3\text{PbI}_3$ / PCBM for different concentrations of Stearic acid.

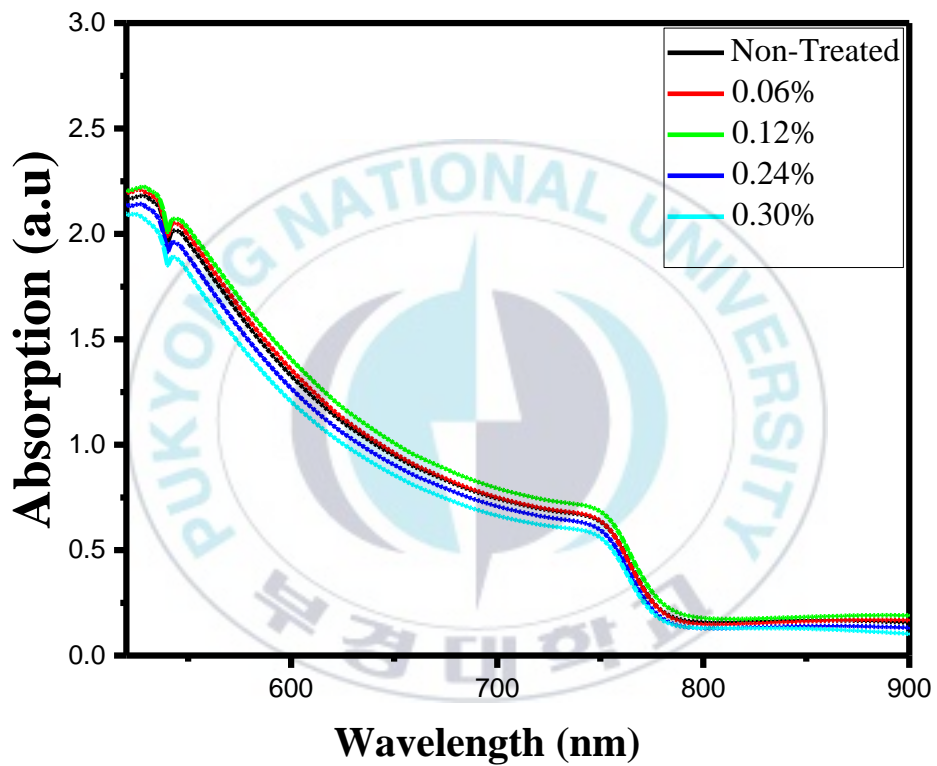


Figure 19. Absorption Spectra of glass/ ITO/PEDOT:PSS/ CH₃NH₃PbI₃/ PCBM for different Ethylenediamine concentrations.

4.6 J-V Characteristics of Treated Devices

The performance of the devices was used to determine the optimum concentrations of both Ethylenediamine and Stearic acid. This was done by varying their concentrations, observing their J-V characteristics from Figure 20 and Figure 21(a-b) as well tabulating their corresponding photovoltaic performances in Table 1 and Table 2. Table 1 shows decreasing photovoltaic performance of the devices for increased Stearic acid concentrations. For instance, concentrations of 10g/ml to 20g/ml correspond to low J_{sc} and poor fill factor, whereas from 8g/ml and below there is a vast improvement in the device performance. The poor performance for concentrations 10g/ml and above, was most likely caused by the layer of Stearic acid being too thick consequently increasing the resistivity of the device. It not only prevents efficient charge collection but also negatively influences the absorption device shown earlier in Figure 18, thus ruling out their practicality for this study. The corresponding J-V curves in Figure 20 show the performance of these devices. From 8g/ml and below the devices exhibited better device performances and an optimum concentration was selected for the best performing device.

In Table 2, it was observed that increased concentrations of Ethylenediamine resulted in reducing efficiencies, mainly due to decreasing V_{oc} and fill factor. The drop in fill factor could be ascribed to the effect of

Ethylenediamine on the quality of the film as mentioned earlier. For a given concentration of Stearic acid however, it was observed that the Voc for all devices remained more or less constant. The relationship between Ethylenediamine and Stearic acid was also studied, thus for a fixed concentration of Stearic acid, Ethylenediamine was varied as before and the photovoltaic parameters tabulated in the same Table.1

Interestingly, it was also observed that increasing the ratio between Ethylenediamine and Stearic acid resulted in better photovoltaic parameters of the treated devices. The best performing device had an efficiency of 15.28%, a Voc of 1.01 V, a Jsc of 20.82 (mA/cm) and a fill factor of 0.72% against a non-treated device of efficiency 16.09%, Voc 1.00 V, a Jsc of 21.92 (mA/cm²) and a fill factor of 0.73%. In addition, no hysteresis was observed in the treated devices as shown in the forward and reverse scan of the J-V slopes in Figure 23. Overall, even after treatment, the advantages of using p-i-n layered devices can be said for our own devices.

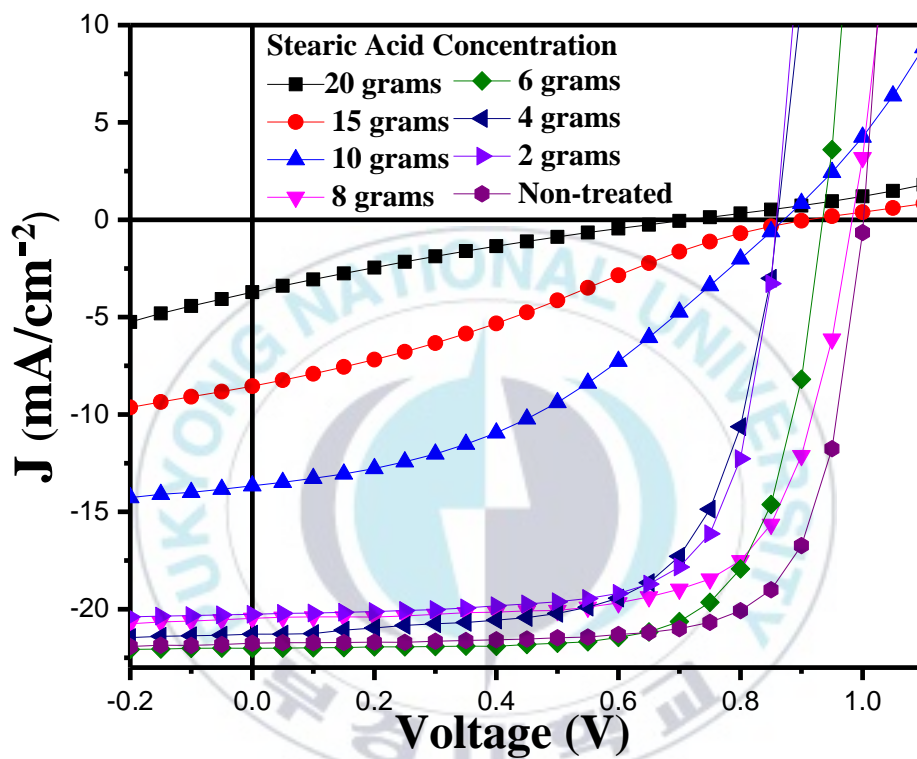


Figure 20. Device performance for varying concentrations of Stearic acid with (0.06%) Ethylenediamine in IPA solution.

Table 1. The table shows the trend in the photovoltaic parameters of different concentrations of Stearic Acid for a) 0% Ethylenediamine (EDA) and b) 0.06% Ethylenediamine in IPA solution.

Stearic acid (g/ml)	EDA (%)	Jsc [mA/cm ²]	Voc [V]	Fill Factor (%)	Efficiency (%)
2	0	20.30	1.00	0.66	13.66
4	0	19.74	0.93	0.74	14.01
6	0	18.65	1.00	0.58	11.27
8	0	20.76	0.99	0.66	13.70
2	0.06	19.09	0.96	0.69	12.74
4	0.06	20.10	1.01	0.67	14.00
6	0.06	19.35	0.97	0.66	12.40
8	0.06	19.56	0.96	0.69	13.11
10	0.06	13.61	0.87	0.39	4.69
15	0.06	8.84	0.91	0.27	2.35
20	0.06	3.71	0.71	0.21	0.56

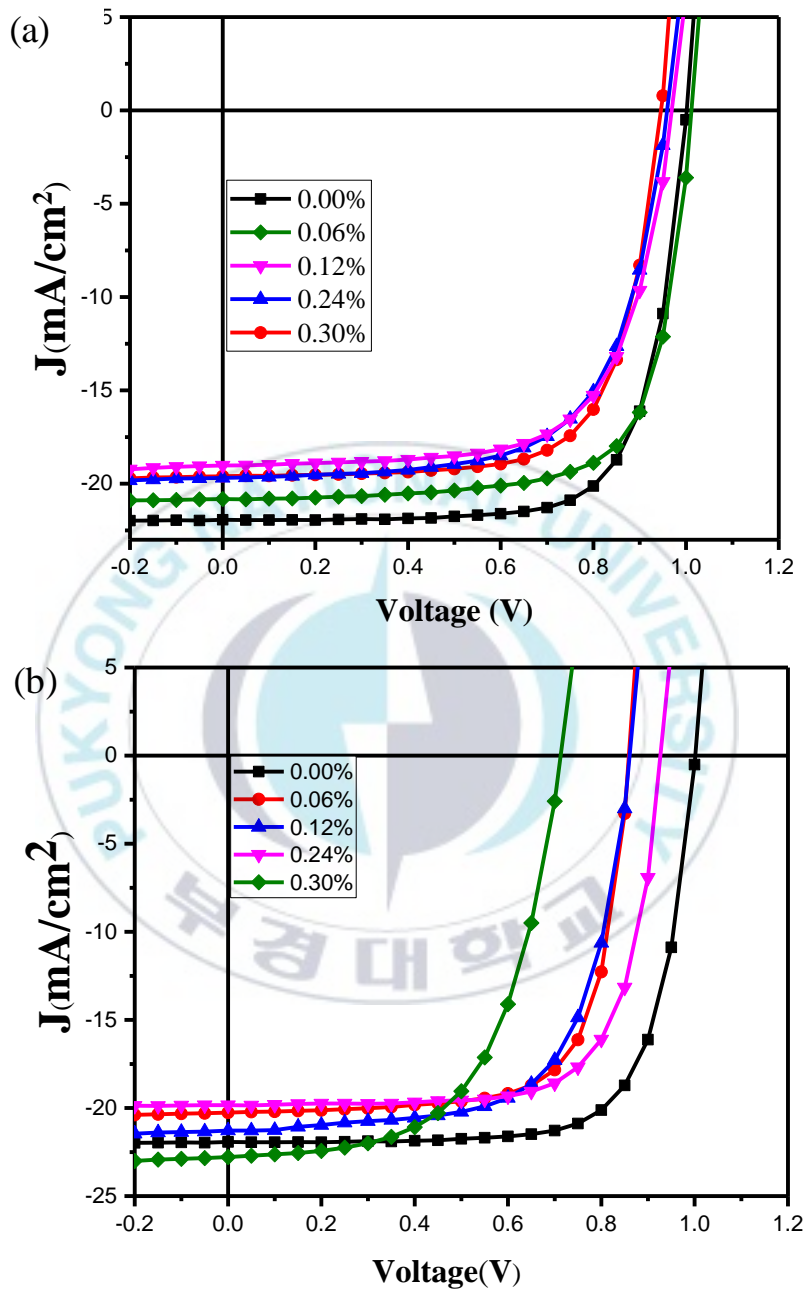


Figure 21. Device performance for different concentrations of Ethylenediamine a) without Stearic acid and b) 6g of Stearic acid coated.

Table 2. The table shows the trend in the photovoltaic parameters of different concentrations of Ethylenediamine for a) without Stearic acid b) 6g of Stearic acid.

Stearic acid (g)	EDA (%)	Jsc [mA/cm ²]	Voc [V]	Fill Factor (%)	Efficiency (%)
0	0.00	21.92	1.00	0.73	16.09
0	0.06	20.20	0.85	0.71	12.48
0	0.12	21.28	0.86	0.66	12.11
0	0.24	19.84	0.93	0.71	13.26
0	0.30	22.78	0.72	0.58	9.52
6	0.06	20.82	1.01	0.72	15.28
6	0.12	19.71	0.96	0.67	12.40
6	0.24	19.60	0.94	0.70	13.00
6	0.30	19.68	0.95	0.65	12.39

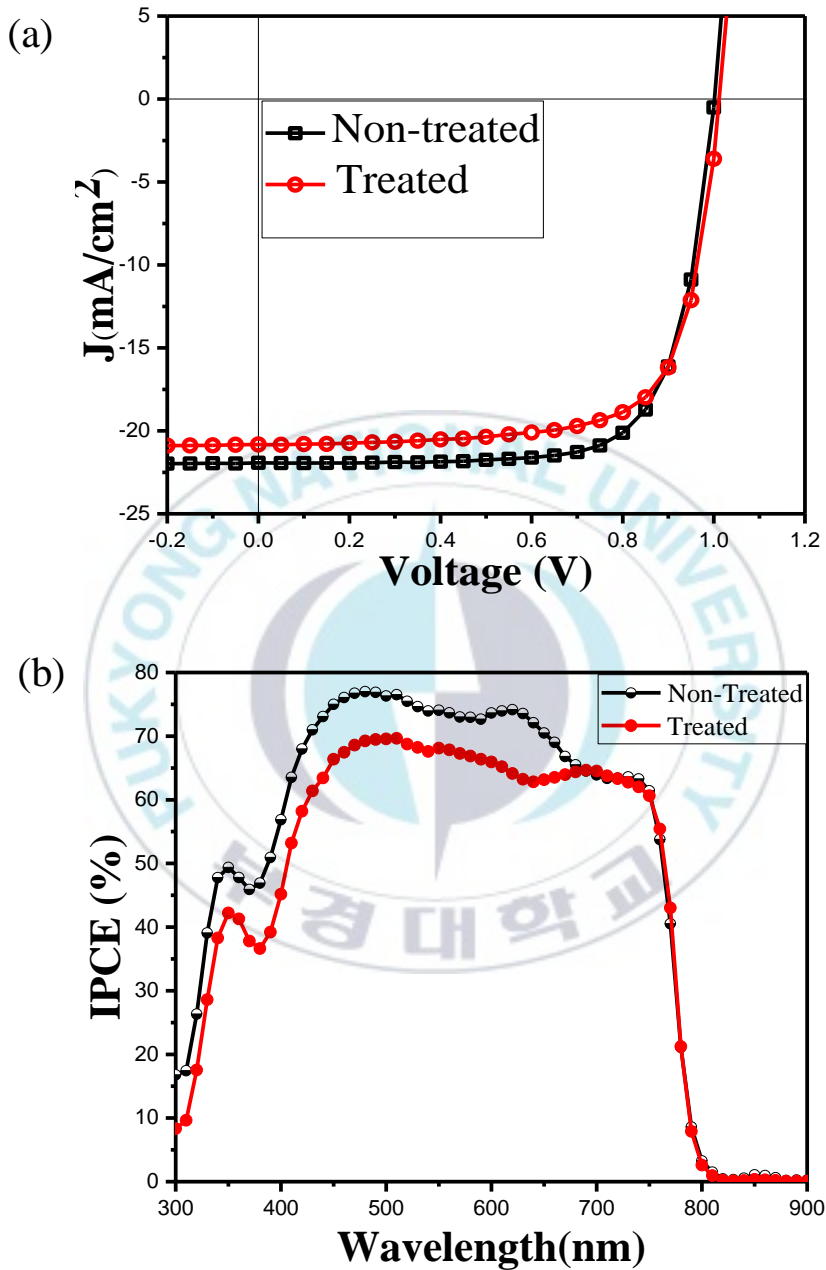


Figure 22. J-V characteristics for a) the best performing treated device vs non-treated device and b) the incident photo-to-current efficiency (IPCE) spectrum for device prepared with different annealing method.

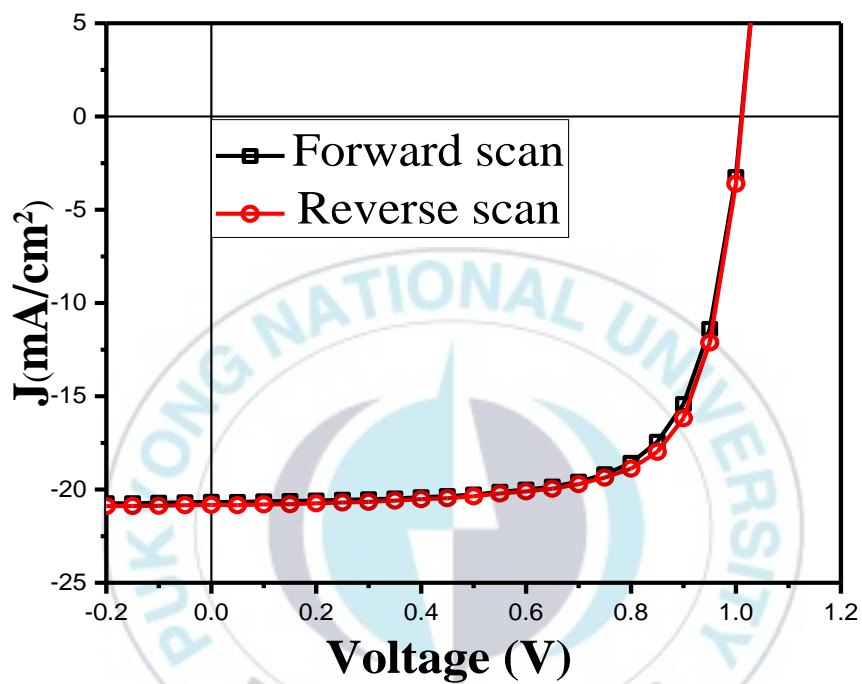


Figure 23. Forward and Reverse Scan for best performing treated device.

4.7 Device Performance in Air

The moisture stability of the treated device was tested by comparing the efficiencies of non-treated and treated devices when exposed to a humid environment. The devices were stored in a dark condition with 40% RH and their efficiencies with time were plotted as shown in Figure 24a and Figure 24b. Two conditions were set up, device efficiencies without electrode redeposition shown in Figure 24a, and with electrode redeposition, shown in Figure 24b. In Figure 24a, we see that treated devices showed better stability in air compared to non-treated devices evidenced by the moderate drop in their efficiencies compared to that of non-treated devices. Whereas the treated device kept nearly 70% of its initial efficiency, the non-treated device only retained 10% of its initial efficiency. After electrode redeposited, treated devices exhibited even longer lifetimes. Their restored devices retained 90% of their initial efficiencies after every redeposition, as shown in Figure 24b.

Furthermore, the J-V curves of the treated devices were characterized for devices exposed to air and then redeposited with the electrode. The J-V curves, Figure 25, show a minor drop in the J_{sc} and V_{oc} , with no S-shaped slope previously seen in the untreated devices. This entails that the treated surface protected the devices from moisture as well as the Aluminium electrode from the perovskite film thus increasing the device lifetime.

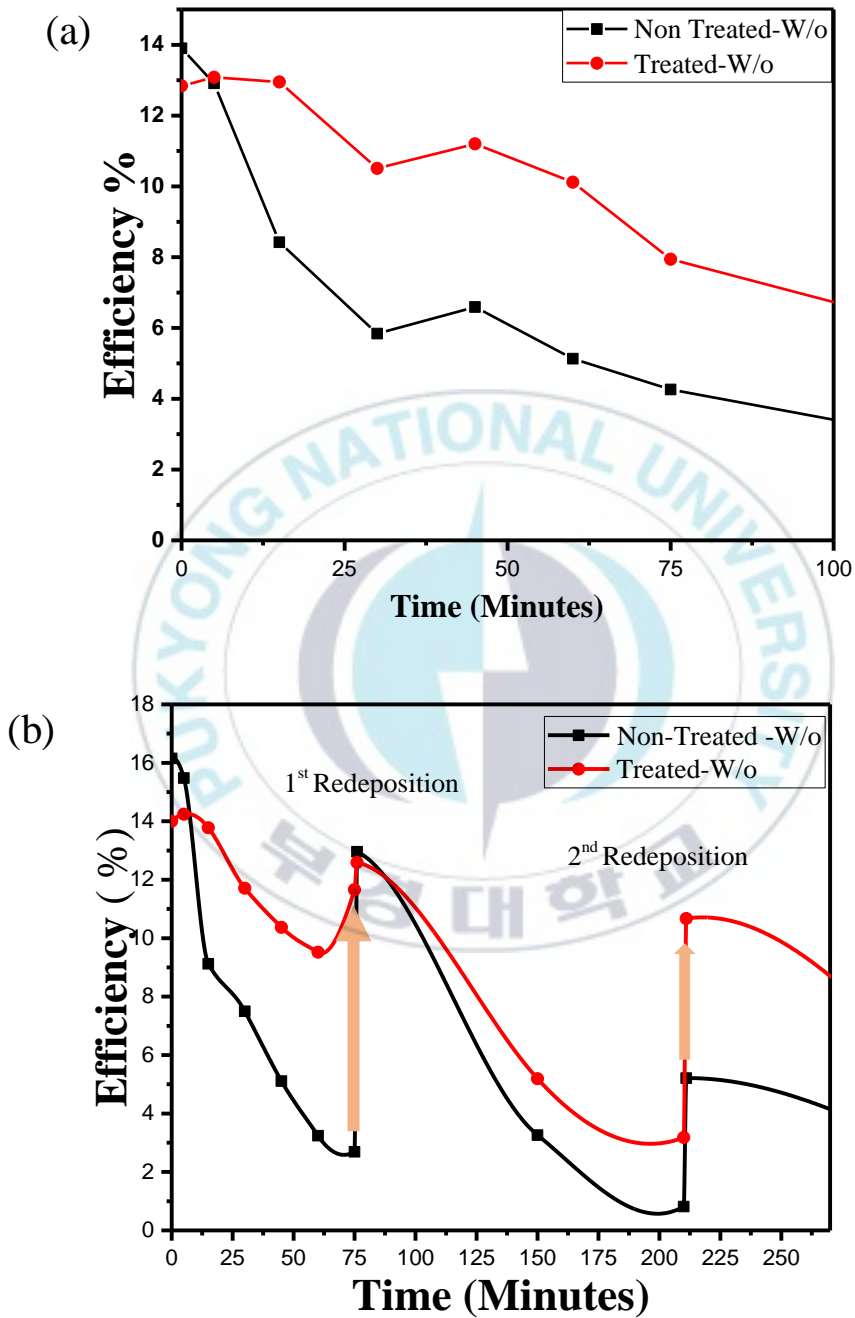


Figure 24. Device efficiency with time for devices stored in dark and humid condition, 40% RH for a) treated and non-treated devices without redeposition, b) with redeposition.

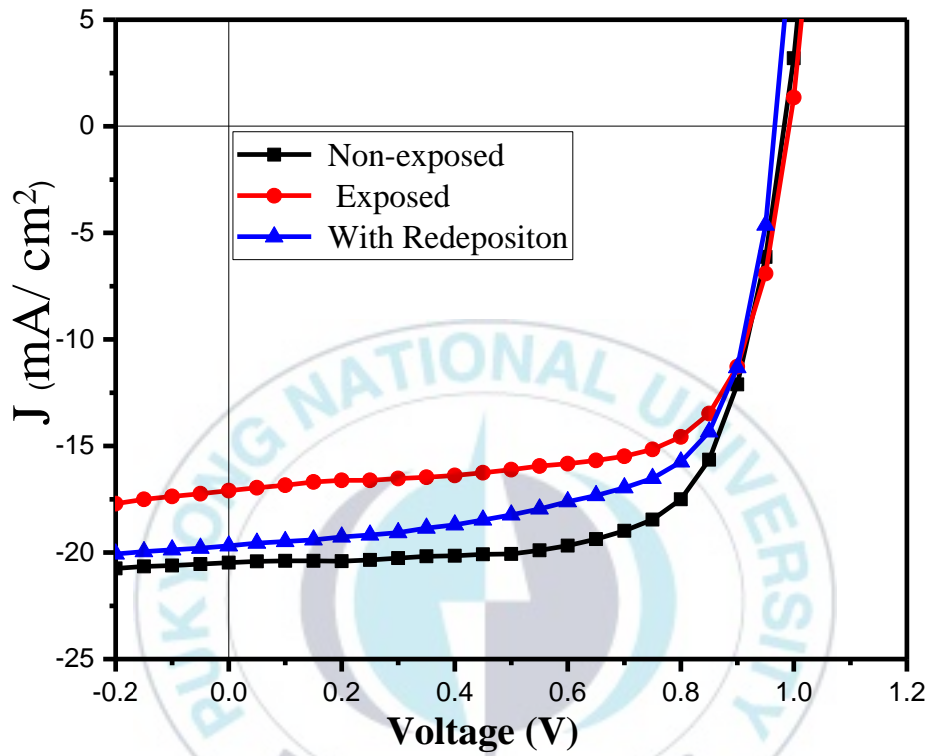


Figure 25. J-V curves of treated devices with and without exposure to dark and humid condition, 40% RH.

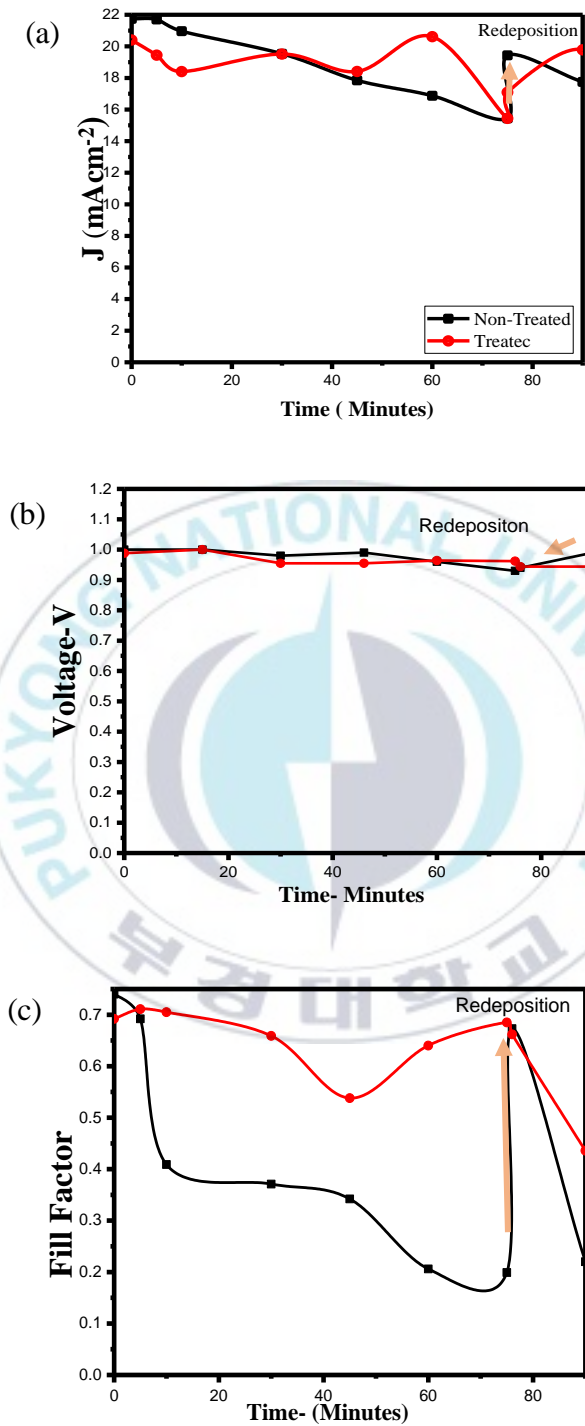


Figure 26. Changes in the photovoltaic parameters a) Jsc, b) Voc and c) fill factor for non-treated and treated devices exposed to air in dark condition with 40% RH, before and after redeposition

Chapter 5. Conclusion

Having made strides with record efficiencies of 22.1%, concern on perovskite solar cells is steered towards their instability in air. Studying and improving the stability of perovskite solar cells brings them a step closer to commercialization. In this study, I begun with identifying a primary source of degradation in our perovskite solar cells. A combination of moisture, the perovskite film and Aluminum electrodes was largely responsible for the rapid drop in efficiencies. A possible degradation mechanism was then suggested to explain the effect of the electrodes on the device. Interaction amongst these factors formed Aluminum Iodide at the electrode rendering it inefficient. However, by replacing electrodes at some time intervals we not only identified a particular stage of degradation in our devices, but also improved their lifetime.

To further improve the device stability, Stearic acid was selected due to its hydrophobic property, to treat the surface of the ETL namely PCBM. After treatment, the contact angle of the film increased and a longer resistance to moisture absorption was observed when the samples were immersed in water indicating that PCBM had improved hydrophobicity. We have also shown that with a PCBM treated layer, devices show enhanced stability when stored in humid conditions, on average, the treated devices retained nearly 80% of

their efficiencies within the first 2 hours of exposure compared to non-treated devices, which only retained 16% of their efficiencies when exposed to a humid condition of 40%.



Reference List

- [1] A. Kojima, K. Teshima, Y. Shirai, T. Miyasaka, *Journal of the American Chemical Society* **2009**, *131*, 6050.
- [2] V. D'Innocenzo, G. Grancini, M. J. P. Alcocer, A. R. S. Kandada, S. D. Stranks, M. M. Lee, G. Lanzani, H. J. Snaith, A. Petrozza, *Nature Communications* **2014**, *5*, 3586.
- [3] H.-S. Kim, S. H. Im, N.-G. Park, *J. Phys. Chem. C* **2014**, *118*, 5615.
- [4] M. Saba, M. Cadelano, D. Marongiu, F. Chen, V. Sarritzu, N. Sestu, C. Figus, M. Aresti, R. Piras, A. G. Lehmann, C. Cannas, A. Musinu, F. Quochi, A. Mura, G. Bongiovanni, *Nature Communications* **2014**, *5*, 5049.
- [5] M. M. Lee, J. Teuscher, T. Miyasaka, T. N. Murakami, H. J. Snaith, *Science* **2012**, *338*, 643.
- [6] Y. Li, W. Yan, Y. Li, S. Wang, W. Wang, Z. Bian, L. Xiao, Q. Gong, *Scientific reports* **2015**, *5*, 14485.
- [7] G. Xing, N. Mathews, S. Sun, S. S. Lim, Y. M. Lam, M. Gratzel, S. Mhaisalkar, T. C. Sum, *Science (New York, N.Y.)* **2013**, *342*, 344.
- [8] C. Wehrenfennig, G. E. Eperon, M. B. Johnston, H. J. Snaith, L. M. Herz, *Advanced materials (Deerfield Beach, Fla.)* **2014**, *26*, 1584.

- [9] S. D. Stranks, G. E. Eperon, G. Grancini, C. Menelaou, M. J. P. Alcocer, T. Leijtens, L. M. Herz, A. Petrozza, H. J. Snaith, *Science (New York, N.Y.)* **2013**, 342, 341.
- [10] S. S. Shin, E. J. Yeom, W. S. Yang, S. Hur, M. G. Kim, J. Im, J. Seo, J. H. Noh, S. I. Seok, *Science (New York, N.Y.)* **2017**, 356, 167.
- [11] N. Ahn, D.-Y. Son, I.-H. Jang, S. M. Kang, M. Choi, N.-G. Park, *Journal of the American Chemical Society* **2015**, 137, 8696.
- [12] J. Burschka, N. Pellet, S.-J. Moon, R. Humphry-Baker, P. Gao, M. K. Nazeeruddin, M. Gratzel, *Nature* **2013**, 499, 316.
- [13] M. Liu, M. B. Johnston, H. J. Snaith, *Nature* **2013**, 501, 395.
- [14] Q. Bao, X. Liu, S. Braun, M. Fahlman, *Adv. Energy Mater.* **2014**, 4, 1301272.
- [15] Y. Bai, Q. Dong, Y. Shao, Y. Deng, Q. Wang, L. Shen, D. Wang, W. Wei, J. Huang, *Nature Communications* **2016**, 7, 12806 EP -.
- [16] J. You, Z. Hong, Y. M. Yang, Q. Chen, M. Cai, T.-B. Song, C.-C. Chen, S. Lu, Y. Liu, H. Zhou, Y. Yang, *ACS nano* **2014**, 8, 1674.
- [17] Y. Liu, I. Shin, I.-W. Hwang, S. Kim, J. Lee, M.-S. Yang, Y. K. Jung, J.-W. Jang, J. H. Jeong, S. H. Park, K. H. Kim, *ACS applied materials & interfaces* **2017**, 9, 12382.
- [18] J. H. Heo, H. J. Han, D. Kim, T. K. Ahn, S. H. Im, *Energy Environ. Sci.* **2015**, 8, 1602.

- [19] M. Jørgensen, K. Norrman, F. C. Krebs, *Solar Energy Materials and Solar Cells* **2008**, *92*, 686.
- [20] X. Lu, Y. Jin, S. Tan, L. Zhang, Y. Liu, X. Zhang, J. Xu, *Journal of Adhesion Science and Technology* **2008**, *22*, 1841.
- [21] M. A. Peña, J. L. G. Fierro, *Chem. Rev.* **2001**, *101*, 1981.
- [22] D. B. Mitzi, *Inorg. Chem.* **2000**, *39*, 6107.
- [23] V. Gonzalez-Pedro, E. J. Juarez-Perez, W.-S. Arsyad, E. M. Barea, F. Fabregat-Santiago, I. Mora-Sero, J. Bisquert, *Nano letters* **2014**, *14*, 888.
- [24] J.-S. Zhou, J. B. Goodenough, *Physical review letters* **2005**, *94*, 65501.
- [25] T. Sato, S. Takagi, S. Deledda, B. C. Hauback, S.-i. Orimo, *Scientific reports* **2016**, *6*, 23592.
- [26] G. King, P. M. Woodward, *J. Mater. Chem.* **2010**, *20*, 5785.
- [27] C. Manspeker, S. Venkatesan, A. Zakhidov, K. S. Martirosyan, *Current Opinion in Chemical Engineering* **2017**, *15*, 1.
- [28] R. J. Sutton, G. E. Eperon, L. Miranda, E. S. Parrott, B. A. Kamino, J. B. Patel, M. T. H?rantner, M. B. Johnston, A. A. Haghighirad, D. T. Moore, H. J. Snaith, *Adv. Energy Mater.* **2016**, *6*, 1502458.
- [29] B. Conings, J. Drijkoningen, N. Gauquelin, A. Babayigit, J. D'Haen, L. D'Olieslaeger, A. Ethirajan, J. Verbeeck, J. Manca, E. Mosconi, F. de Angelis, H.-G. Boyen, *Adv. Energy Mater.* **2015**, *5*, 1500477.
- [30] G. Niu, X. Guo, L. Wang **2015**, *3*, 8970.

- [31] J. M. Frost, K. T. Butler, F. Brivio, C. H. Hendon, M. van Schilfgaarde, A. Walsh, *Nano letters* **2014**, *14*, 2584.
- [32] A. M. A. Leguy, Y. Hu, M. Campoy-Quiles, M. I. Alonso, O. J. Weber, P. Azarhoosh, M. van Schilfgaarde, M. T. Weller, T. Bein, J. Nelson, P. Docampo, P. R. F. Barnes, *Chem. Mater.* **2015**, *27*, 3397.
- [33] E. Mosconi, J. M. Azpiroz, F. de Angelis, *Chem. Mater.* **2015**, *27*, 4885.
- [34] S. Yang, Y. Wang, P. Liu, Y.-B. Cheng, H. J. Zhao, H. G. Yang, *Nature Energy* **2016**, *1*, 15016 EP -.
- [35] J. You, L. Meng, T.-B. Song, T.-F. Guo, Y. Yang, W.-H. Chang, Z. Hong, H. Chen, H. Zhou, Q. Chen, Y. Liu, N. D. Marco, *Nat Nano* **2016**, *11*, 75.
- [36] J. D. Roehling, C. W. Rochester, H. W. Ro, P. Wang, J. Majewski, K. J. Batenburg, I. Arslan, D. M. DeLongchamp, A. J. Moulé, *J. Polym. Sci. Part B: Polym. Phys.* **2014**, *52*, 1291.
- [37] S. A. Mauger, L. Chang, S. Friedrich, C. W. Rochester, D. M. Huang, P. Wang, A. J. Moulé, *Adv. Funct. Mater.* **2013**, *23*, 1935.
- [38] H. Wang, J. G. Hou, O. Takeuchi, Y. Fujisuku, A. Kawazu, *Phys. Rev. B* **2000**, *61*, 2199.
- [39] G. K. Wertheim, D. Buchanan, *Solid State Communications* **1993**, *88*, 97.
- [40] D. L. Matz, E. L. Ratcliff, J. Meyer, A. Kahn, J. E. Pemberton, *ACS applied materials & interfaces* **2013**, *5*, 6001.

- [41] K. Domanski, J.-P. Correa-Baena, N. Mine, M. K. Nazeeruddin, A. Abate, M. Saliba, W. Tress, A. Hagfeldt, M. Gratzel, *ACS nano* **2016**, *10*, 6306.
- [42] G. Zhang, S. A. Hawks, C. Ngo, L. T. Schelhas, D. T. Scholes, H. Kang, J. C. Aguirre, S. H. Tolbert, B. J. Schwartz **2015**, *7*, 25247.
- [43] Y. Kato, L. K. Ono, M. V. Lee, S. Wang, S. R. Raga, Y. Qi, *Adv. Mater. Interfaces* **2015**, *2*, 1500195.
- [44] A. Guerrero, J. You, C. Aranda, Y. S. Kang, G. Garcia-Belmonte, H. Zhou, J. Bisquert, Y. Yang, *ACS nano* **2016**, *10*, 218.
- [45] S. Wang, Y. Jiang, E. J. Juarez-Perez, L. K. Ono, Y. Qi, *Nat. Energy* **2016**, *2*, 16195.
- [46] Y. Hu, J. Schlipf, M. Wussler, M. L. Petrus, W. Jaegermann, T. Bein, P. Muller-Buschbaum, P. Docampo, *ACS nano* **2016**, *10*, 5999.
- [47] H. Tsai, W. Nie, J.-C. Blancon, C. C. Stoumpos, R. Asadpour, B. Harutyunyan, A. J. Neukirch, R. Verduzco, J. J. Crochet, S. Tretiak, L. Pedesseau, J. Even, M. A. Alam, G. Gupta, J. Lou, P. M. Ajayan, M. J. Bedzyk, M. G. Kanatzidis, *Nature* **2016**, *536*, 312.
- [48] X. Li, M. I. Dar, C. Yi, J. Luo, M. Tschumi, S. M. Zakeeruddin, M. K. Nazeeruddin, H. Han, M. Gratzel, *Nature chemistry* **2015**, *7*, 703.
- [49] B. Li, C. Fei, K. Zheng, X. Qu, T. Pullerits, G. Cao, J. Tian, *J. Mater. Chem. A* **2016**, *4*, 17018.

- [50] J. Zhang, Z. Hu, L. Huang, G. Yue, J. Liu, X. Lu, Z. Hu, M. Shang, L. Han, Y. Zhu, *Chemical communications (Cambridge, England)* **2015**, *51*, 7047.
- [51] Q. Wang, Q. Dong, T. Li, A. Gruverman, J. Huang, *Advanced materials (Deerfield Beach, Fla.)* **2016**, *28*, 6734.
- [52] D. Bi, C. Yi, J. Luo, J.-D. Décoppet, F. Zhang, S. M. Zakeeruddin, X. Li, A. Hagfeldt, M. Grätzel, *Nature Energy* **2016**, *1*, 16142 EP -.
- [53] I. S. Kim, D. H. Cao, D. B. Buchholz, J. D. Emery, O. K. Farha, J. T. Hupp, M. G. Kanatzidis, A. B. F. Martinson, *Nano letters* **2016**, *16*, 7786.
- [54] E. M. Sanehira, B. J. Tremolet de Villers, P. Schulz, M. O. Reese, S. Ferrere, K. Zhu, L. Y. Lin, J. J. Berry, J. M. Luther **2016**, *1*, 38.
- [55] D. P. Nenon, J. A. Christians, L. M. Wheeler, J. L. Blackburn, E. M. Sanehira, B. Dou, M. L. Olsen, K. Zhu, J. J. Berry, J. M. Luther, *Energy Environ. Sci.* **2016**, *9*, 2072.
- [56] M. S. Lim, K. Feng, X. Chen, N. Wu, A. Raman, J. Nightingale, E. S. Gawalt, D. Korakakis, L. A. Hornak, A. T. Timperman, *Langmuir the ACS journal of surfaces and colloids* **2007**, *23*, 2444.
- [57] Y. T. Tao, *J. Am. Chem. Soc.* **1993**, *115*, 4350.
- [58] R. W. Corkery, *Langmuir* **1997**, *13*, 3591.
- [59] A. Demirbas, A. Sari, O. Isildak, *Journal of hazardous materials* **2006**, *135*, 226.

- [60] L. Jiang, Y. Zhao, J. Zhai, *Angew. Chem.* **2004**, *116*, 4438.
- [61] X. J. Feng, L. Jiang, *Advanced Materials* **2006**, *18*, 3063.
- [62] C. Su, Z. Lu, H. Zhao, H. Yang, R. Chen, *Applied Surface Science* **2015**, *353*, 735.



Acknowledgements

I would like to give my sincerest gratitude to my supervisor, Professor Park Sung Heum for firstly giving me the opportunity to work under his supervision, to say I have learnt a lot under his instruction is an understatement. His continuous guidance and faith in me gave me more strength and confidence to complete my Master's degree programme. Not only did he instruct me but also inspired me through his passion for Physics and his hard work. I will be forever grateful and humbled that I had the opportunity to be his student.

Secondly, I would like to extend my gratitude to Professor Choi Byung Chun and Professor Jang Jae Won for taking the time out of their busy schedule to review my Master Thesis. Their experience and advice gave me new insight and strengthened the core idea of the paper.

Not only the Professors mentioned above, but also to the Faculty and staff of the Department of Physics and International Students Department here at Pukyong National University, I would like to say thank you for your continued support and mentorship, which made my studies more comfortable.

My gratitude goes to the members of staff of the Department of Physics at the University, notably Dr. H.V Mweene and Mr. Nchimunya Mwiinga who guided me during my undergraduate studies and helped with the application process.

Importantly, I would like to thank the Government of the Republic of Korea through their KGSP Programme for granting me the opportunity to study in their country, a privilege I do not take for granted.

My deepest appreciation goes to the members of the Opto-Electronic Device Physics Lab, Jihoon Lee, Dal Yong Lee, Insoo Shin, Oh Keun Yong, Seungmin Kim, Yong Chao Ma, Yang Liang Yu, Hyeon Seok Yang and Danbi Kim for their patience and willingness to teach me how to work with opto-electronic devices, their effort is what made my work possible. I could not have asked for better lab mates and I hope to work with them in the future.

I would like to thank my family and friends, Pastor and Mrs. Woo, Ms. Yeonhee Cho, who have been with me from the very beginning, sacrificing a lot to see me achieve my goals. I am incredibly blessed to have been surrounded by them.

Finally yet importantly, I thank the Almighty God for having seen me through this programme, he has been my strength through good and hard times.

July 12, 2017

Pesi Mwitumwa Hangoma.